FILE COPY

Simultaneous Wave and Current Forces on a Cylinder Near the Bottom Boundary

DAVID A. KNOLL and JOHN B. HERBICH
Ocean Engineering Program
Civil Engineering Department

TAMU-SG-81-203
COE Report No. 247
May 1981

Texas A&M University Sea Grant College Program

SIMULTANEOUS WAVE AND CURRENT FORCES ON A CYLINDER NEAR THE BOTTOM BOUNDARY

by

David A. Knoll and John B. Herbich

Ocean Engineering Program

Civil Engineering Department

Texas A&M University

College Station, Texas 77843

May 1981

TAMU-SG-81-203

COE Report No. 247

Partially Supported through Institutional Grant 04-7-158-44105

to Texas A&M University

by the Office of Sea Grant

National Oceanic and Atmospheric Administration

Department of Commerce

$5.00

Order from:

Sea Grant College Program
Texas A&M University
College Station, Texas 77843

ABSTRACT

The interaction of waves and currents and their relationship to the forces on submerged pipelines was investigated at Texas A&M University. A model pipeline in a wave-current test facility is used to obtain experimental force values which are compared to values predicted by various theoretical methods of representing wave propagation in a current.

The Morison equation is employed to evaluate the forces on the horizontal cylinder. The major input parameters required by this equation are the water particle kinematics of velocity and acceleration and the coefficients of drag and inertia. Each of these parameters is investigated individually in order to ensure that compensating errors in the force calculations are eliminated. The coefficient of drag is determined from the simultaneous measurements of the horizontal water particle kinematics and the fluid force on the cylinder. Several wave theories for waves propagating in still water are modified to include currents by various combinations of their respective horizontal velocity fields. These water particle kinematics are compared directly to experimentally determined values.

The measured forces are compared to the forces obtained by the Morison equation with the coefficients determined in this study and the kinematics predicted by the modified wave theories. The data are also compared to previous results for the individual cases of waves or currents. These comparisons demonstrate the changes of the coefficients of drag for the combined wave and current conditions.

The primary purpose of this paper is not to provide explicit prototype design criteria, but to provide the design engineer with an insight into the fluid force parameters of interacting waves and currents. The results are presented in a manner that demonstrates the apparent acceptability of superimposing the velocity fields of the wave and current to predict the total velocity field for the determination of the fluid force by the Morison equation.

PREFACE

The research described in this report was conducted as part of the research program in ocean engineering at Texas A&M University. Experimental work was conducted in the Hydromechanics Laboratories and was partially supported by the NOAA Sea Grant Program and the Center for Dredging Studies at Texas A&M University. The manuscript was edited by Dr. Gisela Mahoney and prepared for publication by Ms. Joyce Hyden.

TABLE OF CONTENTS

LIST OF TABLES

LIST OF FIGURES

LIST OF FIGURES
(Continued)

LIST OF FIGURES
(Continued)

LIST OF SYMBOLS

a = Wave amplitude

C = Wave celerity with current

C_o = Wave celerity in still water

C_D = Coefficient of drag

C_D' = Coefficient of drag for waves only

C_g = Group celerity

C_m = Coefficient of added mass

C_I = Coefficient of inertia

D = Cylinder diameter

d = Still water depth

E = Dimensionless difference

f_D = Fluid drag force

f_{DC} = Fluid drag force of current only

f_H = Total horizontal fluid force

f_I = Fluid inertial force

g = Acceleration due to gravity

H = Wave height

h = Water depth

k_o = Wave number for wave in still water

L = Wave length

N_{KC} = Keulegan-Carpenter number

N_R = Reynolds number

n = Frequency

R = Velocity ratio

S_x = Radiation stress

T = Period

U = Current velocity

U' = Modified stream velocity

u = Horizontal velocity

$\dot{u}$ = Horizontal acceleration

u_{calc} = Horizontal velocity calculated by wave theories

u_{max} = Maximum horizontal velocity

u_{mea} = Measured horizontal velocity

u_{tot} = Horizontal velocity of both wave and current

V_p = Probe velocity

x = Horizontal coordinate

z = Vertical coordinate

η = Water surface elevation

θ = Phase angle

ϕ = Velocity potential of combined wave and current

ϕ_1 = Velocity potential of wave

ϕ_2 = Velocity potential of current

$\overline{\phi}$ = Surface density spectrum

ϕ_{VV} = Velocity density spectrum

ϕ_{AA} = Acceleration density spectrum

ρ = Density of fluid

ν = Kinematic viscosity

ω_0 = Wave frequency

ω_1 = Angular velocity of calibration device

INTRODUCTION

Offshore industries have long recognized the importance of underwater pipelines as a vital link for the transmission of materials between onshore and offshore facilities. Although these pipelines are costly at sea, they remain the most feasible and therefore the most economical method for transporting materials continuously over relatively short distances. To ensure their continuous operation, adequate design criteria are required. In some cases, a lack of the necessary information for their design has led to high safety factors, which in turn have increased the cost. Additional information concerning the hydrodynamic loads can help reduce the uncertainty and therefore the cost.

The hydrodynamic loads on an offshore pipeline resting on the bottom are a function of parameters associated with the waves and currents acting near the pipeline. There have been many studies conducted to develop the criteria needed to estimate the hydrodynamic loads imposed by waves and currents. Many of these studies have investigated the effect of these phenomena individually, but to date only limited research has been directed towards evaluating the combined effect. In general, the investigations of the interaction of waves and currents and their effect on the fluid force have been directed toward vertical piles and structures in a random wave field with a current present, but the fluid force of waves in the presence of currents on pipelines has not been directly addressed.

The purpose of this research is to investigate the interaction of waves and currents and its relationship to the forces on submerged pipe-

lines. A model pipeline in a wave flume is used to obtain experimental values, which are compared to values predicted by various theoretical methods of representing waves propagating in a current.

The Morison[1] equation is used to evaluate the forces on a horizontal cylinder resting on the bottom. The two major input parameters required by this equation are 1) the water particle kinematics and velocity and acceleration and 2) the coefficients of drag and inertia. Each of these parameters is investigated individually in order to ensure that compensating errors in the force calculations are eliminated. The coefficient of drag is obtained directly by the simultaneous measurements of the water particle kinematics and the fluid force on the cylinder. The horizontal velocity predicted by Airy and Stokes third order wave theories in still water are combined with a current by the algebraic addition of their respective horizontal velocity fields at a specific elevation. These velocities are compared directly to experimentally determined values. Measured forces are compared to the forces obtained by the Morison equation, using the coefficients determined in this research and the kinematics of the modified Airy and Stokes third order wave theories. The error associated with the algebraic addition assumption is investigated.

Many wave and current orientations are possible in the field, but only the case of a wave propagating in the direction of the current is investigated. It is felt that this orientation will represent the most severe condition that will be experienced in the field. Further investigations will be needed to verify this assumption. In order to determine the individual effect of currents on wave forces, the fundamental problem of monochromatic waves and currents must be evaluated before other effects such as random waves can be attempted.

The primary purpose of this research is not to develop explicit prototype design criteria, but to provide the design engineer with an insight into the parameters governing fluid force in combined wave and current conditions. The parameters for fluid force are affected by the interaction of waves and currents, and the variations of these parameters are presented.

LITERATURE REVIEW

The mechanism by which currents affect surface gravity waves has occupied the thoughts of theoreticians for many years. The early works by Longuet-Higgins and Stewart[2,3] are considered classics. Other investigations by Jonsson, et al.[4] provided the design engineer with a practical knowledge of the wave-current interaction. They presented methods which could be used to predict the changes in wave heights, wave lengths, and celerities for a wave propagating in a current. Many more investigations followed. The majority were theoretical studies of the interaction processes. Some researchers, such as Hales and Herbich[5], experimentally measured the changes in wave parameters to contribute a further understanding of the interaction phenomenon.

Recently, the investigations of the wave-current interaction problem have been expanded to consider the effect of this interaction on predictions of the forces on submerged structures. Dalrymple[6], using methods which he had developed previously, analyzed the field data of "Wave Project Two." He determined that the coefficients required by the Morison equation were biased due to the wave-current interaction, so that error could be introduced if this effect was ignored for fluid force calculations.

Considerable work has been accomplished by Tung and Huang[7,8] who investigated the effect of wave-current interaction on random wave fields. They developed an expression which includes a current when computing an energy spectrum for a given wind speed. Including a current will change the energy of a given random wave field, and therefore the response of a

structure to this wave field will change.

The effect of currents on the forces on submerged pipelines has not received the same degree of attention as have other submerged structures. There has been an abundance of research on submerged pipelines concerning only the condition of wave forces. In these investigations, the effect of roughness, distance from the boundary, and angle of incidence of the approaching waves have been investigated to determine the coefficients required by the Morison equation. The changes in these coefficients due to the interaction of waves and currents are the main focus of this research.

Longuet-Higgins and Stewart[2] studied the changes in the form of short gravity waves on long waves (such as tides) and currents. Short gravity waves, when superimposed on much longer waves, have a tendency to become both shorter and steeper at the crests of the longer waves, and longer and lower in the troughs. The changes in the amplitude and wavelength of the shorter wave train were rigorously calculated. The results differed essentially from those previously predicted by Unna[9]. Unna showed that the reduction in wavelength when waves meet an adverse current causes a reduction in their celerity and the speed of their energy propagation through the water. He assumed the period of the waves with reference to a fixed point in space is constant and derived an expression for the new wave celerity as:

$$\frac{C}{C_o} = \frac{1}{2} \tanh \frac{2\pi d}{L} \left(1 \pm \sqrt{1 + \frac{4U}{C_1} \coth \frac{2\pi d}{L}}\right) \quad \ldots\ldots\ldots\ldots\ldots\ldots (1)$$

where C is celerity of the wave in the presence of a current of intensity U, and C_o is the celerity of the wave in still water. Unna assumed that the wave energy is propagated at the group celerity plus the speed of the

current. Based on this assumption, in deep water when $U = -\frac{1}{4} C_o$ the net group celerity is equal to zero and no energy can be transmitted, so that the wave must break. These assumptions by Unna stated that there could be no interaction between the wave and current. Longuet-Higgins and Stewart later developed an expression which include an interaction term designated as "the radiation stress." It was shown that when a train of gravity waves of amplitude "a" ride upon a steady current U, the transfer of energy across any vertical plane normal to the motion is the sum of four terms:

$$EC_g + EU + S_x U + \frac{1}{2} \rho h U'^3 \quad \ldots\ldots\ldots\ldots\ldots\ldots\ldots\ldots\ldots\ldots \quad (2)$$

where E denotes the mean energy density, C_g denotes the group velocity and U' is a modified stream velocity. S_x is given by:

$$S_x = E \left(\frac{2C_g}{C} - \frac{1}{2}\right) \quad \ldots\ldots\ldots\ldots\ldots\ldots\ldots\ldots\ldots\ldots\ldots\ldots \quad (3)$$

The first term of equation (2) is the transport of energy of the group velocity, and the second term represents the bodily transport of the free-stream velocity. The last term of equation (2) represents the transport by the stream U of its own kinetic energy. The third term $S_x U$ represents the work done by the current U against the "radiation stress" of the waves. These results were applied to develop relationships for the changes in amplitude and wavelengths for short gravity waves moving on a current or long tidal waves.

Peregrine[10] states that an appreciable error can be introduced because of the significant difference in the dispersion relations for waves propagating on still water and waves propagating on a uniform current. Airy theory was used as a basis to determine the dispersion relationships for both conditions. These two conditions differ, since a wave propagating

on a current has a different celerity due to the interrelationship of the wave number, position vector, and uniform current for the combined condition. Peregrine expanded the graphical technique of Jonsson[4] to determine the solution of dispersion relationships for the combined condition. The difference between the dispersion relations of a wave in still water and wave on a current can be an appreciable source of error if the presence of the current is overlooked. These errors are greatest when relationships among the wave properties at the surface (such as measurements of surface profiles) are used to determine bottom particle kinematics. An example of this type of error is the determination of surface amplitudes from bottom pressure measurements. The minimum period of waves for which a current of 0.5 m/sec (1.65 ft/sec) may be ignored in calculating surface amplitudes from bottom pressure measurements (as calculated by Peregrine[10]) is presented in Table 1.

Table 1 - Minimum period of waves for which a current of 0.5 m/sec (1.64 ft/sec) may be ignored in calculating surface amplitudes from bottom pressure measurements.[10]

	Depth (m)				
	1	2	5	10	100
Period with error of 5% (sec)	4.5	5.4	6.9	8.0	14.0
Period with error of 20% (sec)	2.7	3.2	4.3	5.3	11.0

Generally, forces on submerged structures are computed from kinematics determined from surface characteristics. Peregrine states that these computed kinematics will be in error; therefore, the calculated forces will be affected by this error.

Dalrymple[11] developed a numerical model for waves propagating on shear currents. He used a bi-linear and linear model to represent ocean

currents. These models represent an extension of the Stream Function theory described by Dean[12], which generates a wave propagating on a current with a velocity profile which is constant in magnitude over the depth. Dalrymple stated that using a shear current model better represents the actual conditions in the ocean. He also stated that one further advantage of these models is that they converge directly on a desired wave height. To develop these models, he had to use several simplifying assumptions. First, he assumed the effect of viscosity could be neglected over short periods of time so that the current profile is well established; secondly, he assumed that the directions of the waves and currents were the same; and thirdly, he assumed the wave to be periodic in space and time. The last assumption neglects any interaction between wave and current because the interaction would cause changes in wave amplitude and wavelength. He compared the results of his model to results obtained by direct superposition of the velocity profile due to a wave in still water and the velocity profile of a current. From these comparisons he concluded that direct superposition of independent velocity fields is not valid because of nonlinear interactions of wave and current. However, in deep water, the errors of superposition are very small.

Jonsson, et al.[4] presented theoretical results of a study of the interaction among surface gravity waves and a steady current. They assumed irrotational flow and a second order Stokes wave motion to introduce the concept of the "mean energy level" for periodic wave motion with a steady current superimposed. This concept can be used to solve the dispersion relationship of a wave propagating in a current. They presented a simple graphical technique which allows using this concept to predict both the wavelength and the wave height for waves in the presence of currents.

There have been several investigations by different authors, who studied experimentally the interaction of waves and currents. One such study was conducted by Sarpkaya[13]. The main objectives of his work were a) to determine the conditions of stability of progressive, oscillatory gravity waves in water flowing over smooth and artifically roughened surfaces, and b) to evaluate the combined effect on the wave propagation of various interrelated characteristics of flowing water, such as viscous shear, turbulent mixing shear, and nonuniform velocity distributions. From the tests, conducted in a wave flume, Sarpkaya concluded that for a given flow, there is only one neutrally stable wave. All other waves show either exponential damping or amplification during their propagation along the channel. He presented a graphical method for determining this neutrally stable wave for various wave and current parameters. He also concluded that the characteristics of waves propagated in flowing water are not identical with those propagated in still water. Thus, the principle of superposition is not applicable.

One of the first three-dimensional tests on the interaction of waves and currents was conducted by Herbich et al.[14] to determine the attenuation of waves by a jet-induced current. This process is referred to as a hydraulic breakwater in technical literature. The study aimed to provide an indication of the area that would be protected by the hydraulic breakwater, and the effectiveness of such a system for wave attenuation. Experimental data are presented in figures that show numerical values of wave attenuation in the protected zone. The conclusions indicate that the current discharge requirements depend upon wave characteristics such as length, height and water depth. For high values of attenuation, higher current velocity is required for steep waves; however, the efficiency is much higher for steep waves than for flat waves.

Additional three-dimensional tests were conducted at the Waterways Experiment Station by Hales and Herbich[5] to investigate the effect of currents on waves in a tidal inlet. They investigated the manner in which nonuniform currents affect the characteristics of a superimposed surface-gravity wave train. The work was conducted in a three-dimensional wave basin which simulated a tidal inlet. Nonuniform currents could be created in both an ebb and flood direction. The current was required to build up on its own accord from essentially zero at the ocean, to a maximum at the inlet throat, to zero again in the bay. From the test results, it was concluded that the changes in the wave parameters due to interaction processes were dependent on the current parameters as expected, but the interaction also was dependent on other parameters such as the water depth and wave steepness. The results of the investigation were presented graphically as a function of various wave and current parameters.

The effects of interacting waves and currents were extended to fluid force determination on submerged structures by Dalrymple[6], who investigated the field data of "Wave Project Two." The data of "Wave Project Two" were from full-scale tests in the Gulf of Mexico. These data included the force on a test structure during Hurricane Carla. It has been estimated that during this hurricane currents as high as .762 m/sec (2.5 ft/sec) should have been experienced. This current would have had a significant effect on the measured wave forces. Three particular aspects of the wave-current interaction problem were investigated: 1) the effect of a mean current in biasing the drag coefficient required by the Morison equation; 2) the approximate determination of mean currents from wave force data; and 3) the effect of wave and current direction on the forces. Dalrymple presented the methods and results of

Aagaard and Dean[15] for the coefficients of drag and inertia without including the effects of the current. These results are shown in Figures 1 and 2. Dalrymple assumed that the inertia coefficient would not be affected by the current, and that the current was in the same direction as the wave. With the above assumptions, Dalrymple derived the following expression for the relative error in the coefficient of drag (C_D) as a function of the ratio of the current velocity (U) to the wave-induced velocity ($\hat{u}$):

$$\frac{C_D' - C_D}{C_D} = \frac{64}{9\pi}\left(\frac{U}{\hat{u}}\right) + \frac{4}{3}\left(\frac{U}{\hat{u}}\right)^2 \quad \ldots\ldots\ldots\ldots\ldots\ldots\ldots\ldots\ldots\ldots \quad (4)$$

where C_D' = drag coefficient determined without including the effect of the current. This expression is presented graphically in Figure 3 as the upper curve. The error, at least for currents in the direction of the waves, is always positive, which indicates that the drag coefficients obtained without assuming a current are larger than the real C_D value. Dalrymple then took another approach to the problem. He computed the drag coefficients by averaging force over the period to determine the zero-force condition. He then computed the relative error in C_D associated with using this averaging process, and presented this error in Figure 3 as the lower curve. Dalrymple concluded that if the effect of the current was not included in the drag coefficient, the value of these coefficients would be greater than the real values, and that the coefficients determined by including the currents are only applicable to the same design situation. He developed a technique that would allow for a determination of the mean current from the force data by minimizing the squared error in the wave forces. He concluded that currents flowing in directions other than the wave direction will result in reduced wave loadings

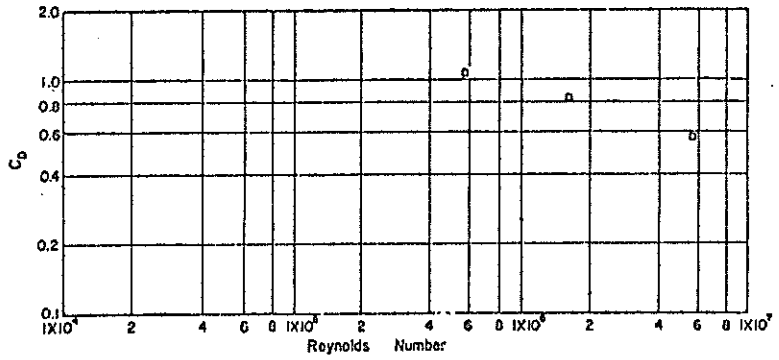

Figure 1 - Drag Coefficients Obtained by Dean and Aagaard by Least Squares Procedure Using Wave Project Two Data [15]

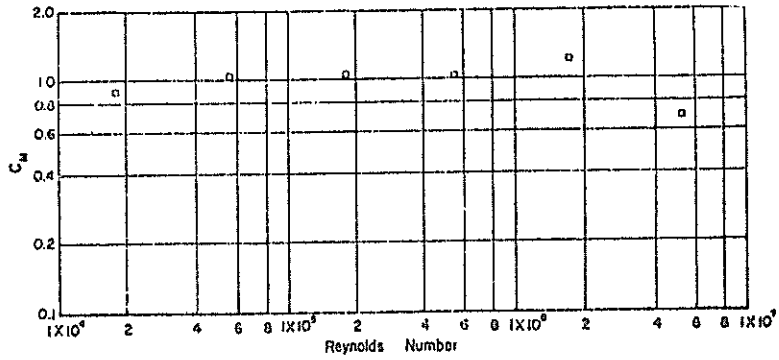

Figure 2 - Inertia Coefficients Obtained by Dean and Aagaard by Least Squares Procedure Using Wave Project Two Data [15]

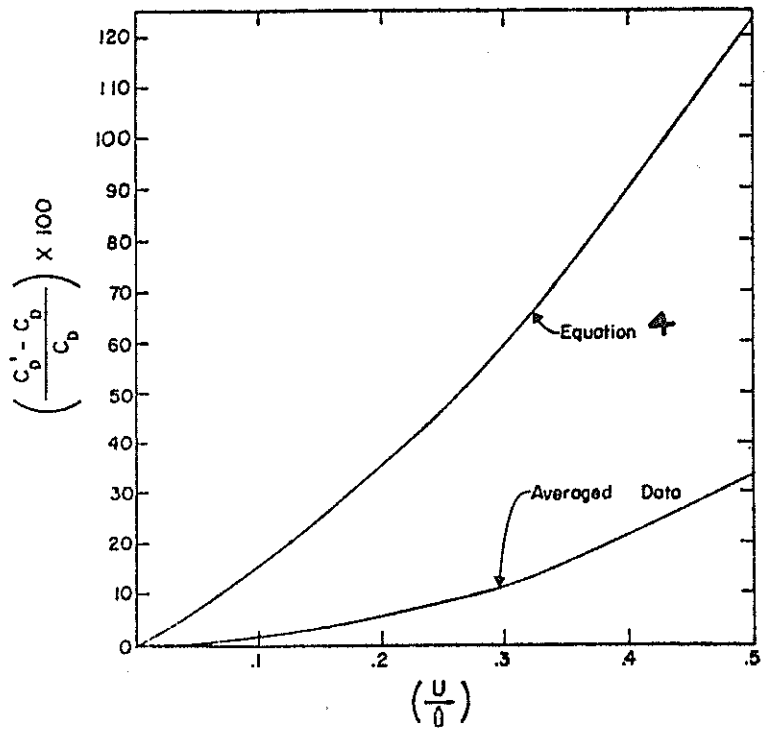

Figure 3 - Percentage Error in Drag Coefficient As A Function of Relative Current Velocity by Linear Analysis [6]

on the structure. Dalrymple states "For relatively small currents in drag-dominated cases, the in-line component of the current is important in modifying the wave form and increasing (or decreasing) the total force."

Tung and Huang[7,8,16] investigated the effect of currents on the statistical properties of waves. An expression for the frequency spectrum of a random wave field was derived based on the Kitaigorodskii-Pierson-Moskowitz spectrum using small amplitude wave theory. The expression for the combined spectrum is

$$\phi(n) = \frac{4\phi_o(n)}{(1 + (1 + \frac{4Un}{g})^{\frac{1}{2}})\ ((1 + \frac{4Un}{g})^{\frac{1}{2}} + (1 + \frac{4Un}{g}))} \quad \ldots\ldots (5)$$

in which n = frequency; g = gravitational acceleration; U = current speed; and $\phi_o(n)$ = frequency spectrum of the waves without the influence of the current. The surface elevation spectra, velocity spectra, and acceleration spectra for a 40 mph wind are shown in Figures 4-6, respectively, for various current speeds. They were determined using the relationship in equation (5).

These results were extended to the dynamic response of a structure under the influence of waves and currents by Wu and Tung[17]. The Morison equation was used to compute the hydrodynamic forces. Four structures were used for the dynamic analysis using an ideal lumped-mass system in conjunction with the normal-mode technique. The method of analysis was a standard method except for the fact that the kinematics of the water motion were determined by the vector summation of the current velocity and the wave-induced velocity. This assumption was introduced into the equations of motion through the linearization of the Morison equation as proposed by Malhotra and Penzien[18]. The equations of motion were solved for the four structures using the normal-mode superposition technique.

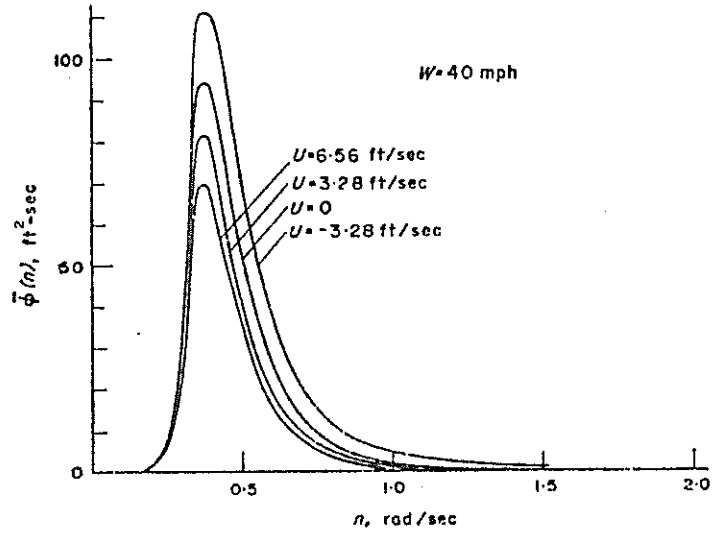

Figure 4 - Surface Spectra [7]

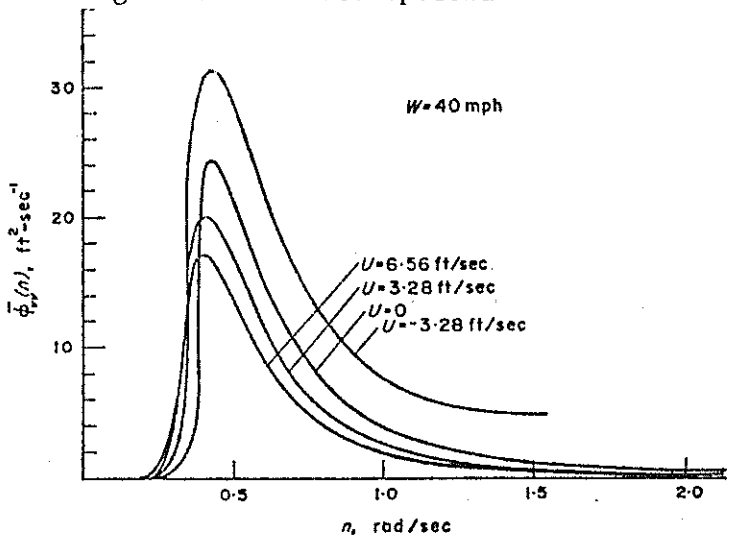

Figure 5 - Velocity Spectra [7]

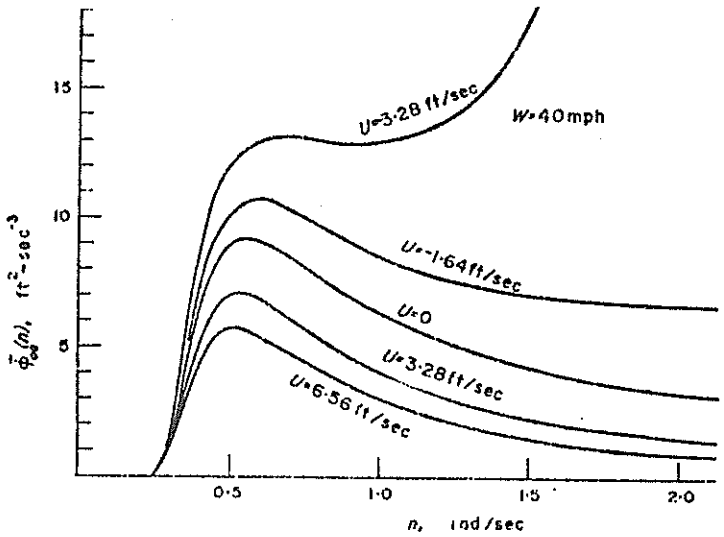

Figure 6 - Acceleration Spectra [7]

Using the technique described above, four structures were investigated for varying wind and current conditions. Three different wind conditions of 50, 75 and 100 ft/sec were used as input to the Pierson-Moskowitz wave spectrum to determine an expression for the random sea state. These wind conditions were applied with a current of either 1, 2, 3 or 4 ft/sec to determine the forces on the structures. The resulting maximum displacements for each of the conditions were compared to explain the effects of currents on the response of the structures.

The main result of this study was that the influence of a current on structural response is significant, especially when the structure is tall and flexible; however, the effect of the current is smaller when the wave forces due to the wind become larger. There seemed to be a large increase in the displacements due to the base shears and overturning moments. This is probably due to the additional force of the current. Wu and Tung leave out two important facts by their assumptions. The first is that the particle motion can be explained by the direct vector addition of the waves and currents. This assumes that there is no interaction between the waves and currents causing some modifications to the momentum. The point that some changes can be expected because of this interaction is noted, but documentation of this fact is still needed. Secondly, the authors made no mention of how the values of C_D and C_m were chosen. The values of C_D and C_m may not be the same for interacting waves and currents. This may be a reasonable assumption, but verification is still needed.

Sekita[19] experimentally determined the coefficients of drag and inertia for a fixed platform structure. He simulated the current by towing a model of the structure in a test tank where waves were being generated in still water. He determined that the additional force of the current

could be directly added algebraically to the wave forces without a current. Since the waves were propagating in still water, the principle of superposition should be valid. This way of representing the current does not, however, represent the interacting process of the waves and currents.

The effect of the current-wave forces interaction has been studied less extensively on submerged pipelines than on other submerged structures such as vertical piles. Much work has been completed on the case of individual wave forces on offshore pipelines and the coefficients required by the Morison equation for this configuration. A report by Davis and Ciani[20] reviewed the present (1976) design aids for determining the fluid force on submerged pipelines. Their main thrust was to present the literature associated with determining the fluid force on the pipeline due to wave forces. Results from many authors were presented and compared. Much of the literature reviewed concerned the determination of coefficients of drag and inertia used in the Morison equation. Several graphs are presented to determine the coefficients of drag and inertia for various wave parameters such as the Reynolds number and the period parameter suggested by Keulegan and Carpenter[21]. Davis and Ciani concluded from their review that the Morison equation has been broadly accepted as reasonable for design and that the velocity and accelerations predicted by Airy wave theory are adequate for the prediction of the kinematics for use in wave force estimates despite its limitations. Also, they concluded that the empirical estimates of the wave force coefficients are for the most part determined in the laboratory and their extension to prototype design is questionable because of scale effects and inconsistencies among the data for the coefficients as presented by different authors. Davis and Ciani presented methods by which the fluid force

could be determined if a current were present, but made no recommendation for a procedure when both waves and currents were present.

Many additional studies have evolved recently on the wave forces on submerged pipelines. In these studies for the most part, the Morison equation or a modified Morison equation is used to calculate the wave forces. The thrust of the current literature is to determine the coefficients of drag and inertia at high Reynolds numbers, which are most representative of the prototype conditions. This type of research is needed, but it also is necessary to expand the knowledge of the drag force coefficients for offshore pipelines under the combined wave-current condition, which is the objective of this research.

THEORETICAL CONSIDERATIONS

The definition sketch of the idealized two-dimensional wave-current problem for offshore pipelines is given in Figure 7. This configuration may represent a pipeline resting on the ocean bottom. The cylinder has both horizontal and vertical forces acting on it due to the passing wave and current. Only the horizontal force is investigated in this research.

Generally the Morison[1] equation is used to predict the horizontal forces on a cylinder resting on the bottom. The limitations of the wave characteristics on the applicability of the Morison equation are best described by Figure 8 (From Garrison and Rao[22]). The areas of applicability are described in terms of two dimensionless parameters. This figure shows that for small ratios of the diameter to wavelength and large ratios of wave height to diameter (H/D), the Morison equation is valid and drag forces are the predominant forces. Typical values for the H/D and D/L ratios for this research are 5.0 and 0.02, respectively. These values indicate that the Morison equation is valid for the fluid force prediction in this research for waves and is assumed to be valid for the combined wave-current condition.

The Morison equation considers the total horizontal force (f_H) as the sum of the horizontal drag force (f_D) and the horizontal inertial force (f_I) (all forces expressed per unit length of cylinder):

$$f_H = f_D + f_I \quad \ldots\ldots\ldots\ldots\ldots\ldots\ldots\ldots\ldots\ldots \quad (6)$$

The drag force is a function of both a drag coefficient (C_D) and the horizontal component of the water particle velocity (u) if the structure

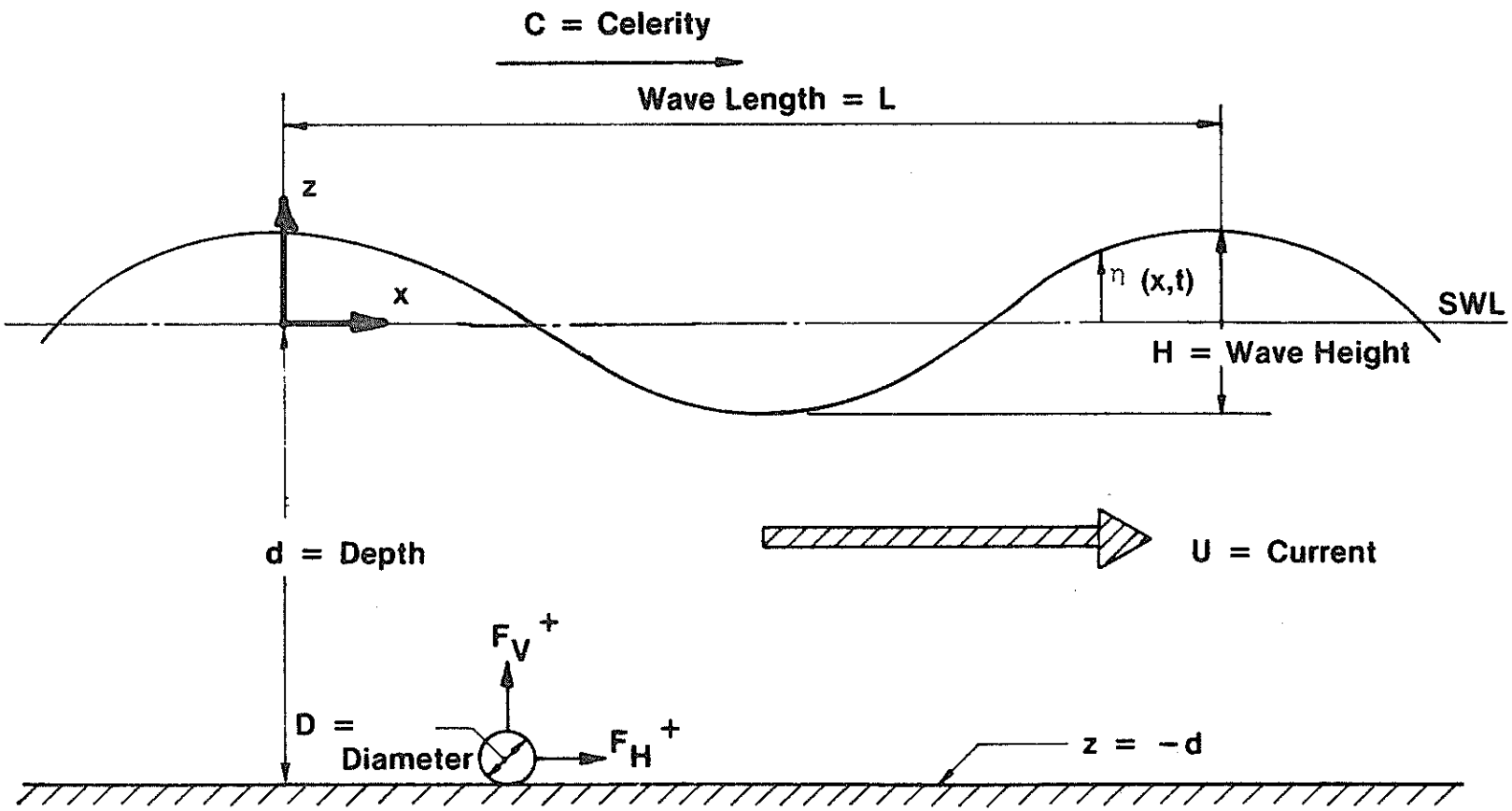

Figure 7 - Definition Sketch of the Pipeline Problem

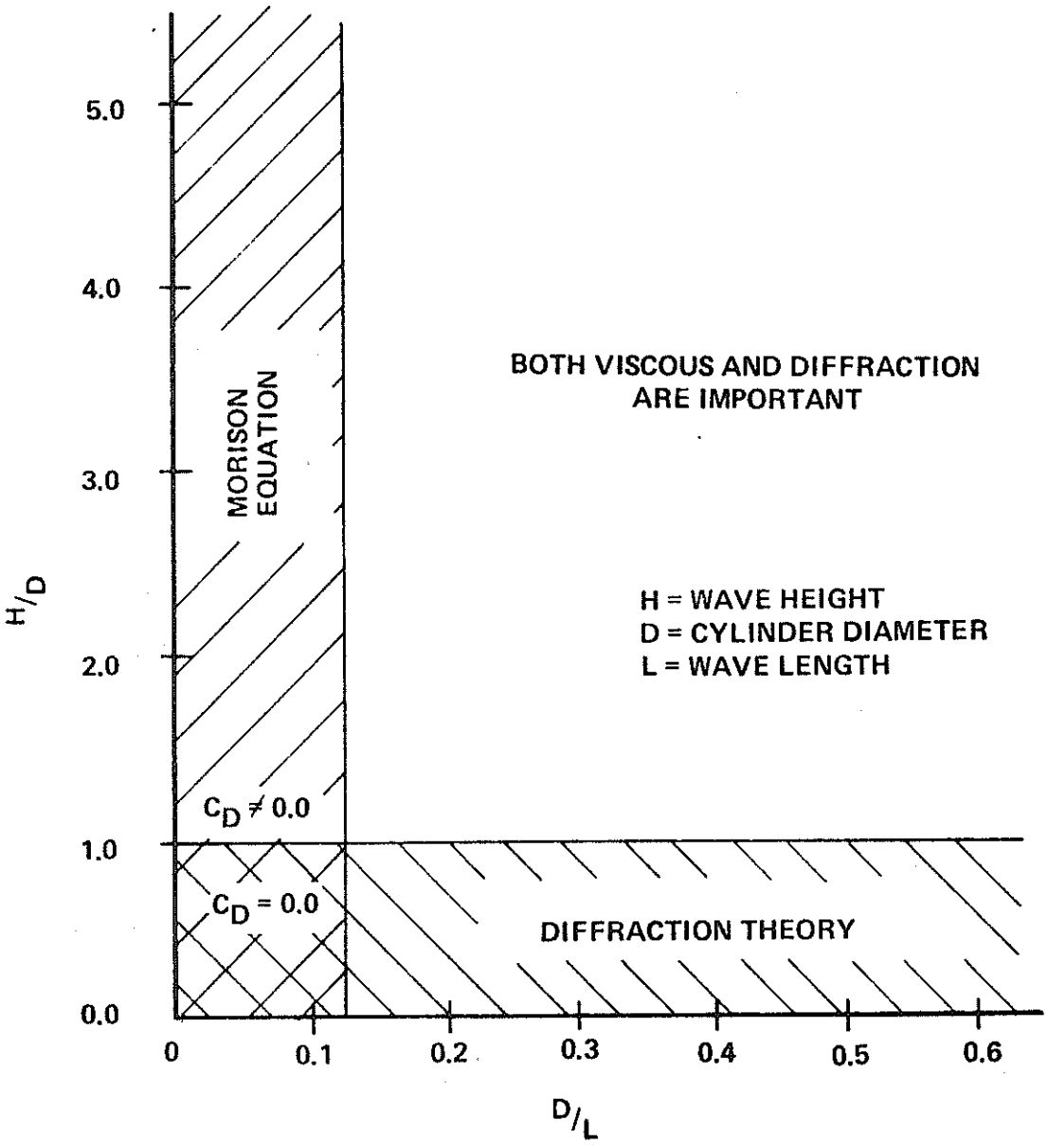

Figure 8 - Regions of Applicability of the Morison Equation and Diffraction Theory with Respect to the Relative Size Parameter (D/L) and the Relative Displacement Parameter (H/D)[22]

were absent or:

$$f_D = \frac{C_D}{2} \rho D\, u|u| \quad \ldots\ldots\ldots\ldots\ldots\ldots\ldots\ldots\ldots\ldots\ldots\ldots\ldots\ldots (7)$$

where D = the diameter of cylinder,

ρ = mass density of the fluid.

The inertia force is a function of the inertial coefficient (C_I) and the horizontal particle acceleration ($\dot{u}$), or:

$$f_I = C_I \frac{\rho \pi D^2}{4} \dot{u} \quad \ldots\ldots\ldots\ldots\ldots\ldots\ldots\ldots\ldots\ldots\ldots\ldots\ldots\ldots (8)$$

To clarify terms, the coefficient of inertia includes a coefficient of added mass (C_m) and a pressure coefficient equal to the pressure acting on an imaginary cylinder in an accelerated flow field divided by the displaced mass of the fluid. For a uniformly accelerated flow, this pressure coefficient is equal to 1.0, thus:

$$C_I = 1.0 + C_m \quad \ldots\ldots\ldots\ldots\ldots\ldots\ldots\ldots\ldots\ldots\ldots\ldots\ldots\ldots (9)$$

Two of the major input parameters required by the Morison equation are the coefficients of drag and inertia. These coefficients must be determined experimentally. This is accomplished by measurements or theoretical predictions of the horizontal water particle kinematics in conjunction with fluid-force measurements. The coefficient of drag can be determined when the horizontal acceleration equals zero by the following equation:

$$C_D = \frac{2f_D}{\rho D\, u|u|} \quad \ldots\ldots\ldots\ldots\ldots\ldots\ldots\ldots\ldots\ldots\ldots\ldots\ldots\ldots (10)$$

when $f_I = 0$. Figure 9 shows qualitatively the local fluid velocities and accelerations for the wave condition and for the combined wave-

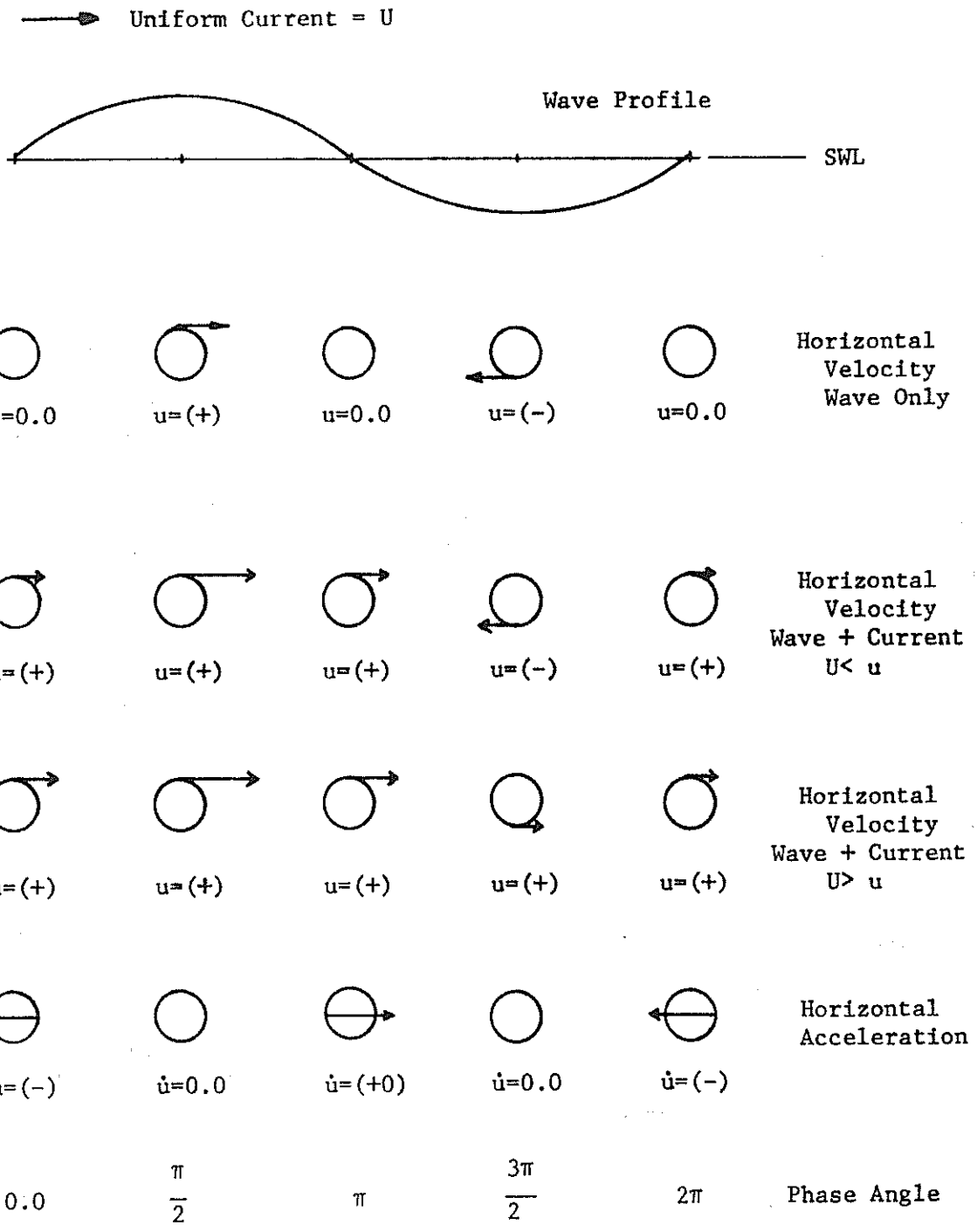

Figure 9 - Local Fluid Velocities and Accelerations for Wave and Wave-Current Conditions

current condition in a Lagrangian reference frame. It can be seen from this figure that under the crest and trough, the horizontal acceleration equals zero.

Likewise, the coefficient of inertia can be determined when the horizontal velocity is equal to zero by the following equation:

$$C_I = \frac{4f_I}{\rho \pi u D^2} \quad \text{.......................... (11)}$$

when $f_D = 0$. These points are well defined for the wave only condition as seen in Figure 9; but for the combined wave-current condition, these points are not well defined because the horizontal velocity does not equal zero. An assumption is made that at phase angles of 0, π, the total force, is the sum of the drag force due to the current and the inertial force due to the wave. To calculate the coefficient of inertia, a drag force due to the current velocity at that elevation (f_{DC}) is subtracted from the total force, so that the resulting force is only due to the acceleration of the wave, or:

$$f_I = f_H - f_{DC} \quad \text{.......................... (12)}$$

The inertia force determined by equation (12) is used to determine the inertia coefficient in equation (11). The coefficients of drag and inertia are generally presented as functions of two dimensionless parameters. The first parameter is the Reynolds number (N_{RE}). The Reynolds number can indicate the dimensionless ratio of the inertial forces to the viscous forces in fluid motion, or:

$$N_{RE} = \frac{Du}{\nu} \quad \text{.......................... (13)}$$

where D = characteristic length (diameter)

u = horizontal component of the particle velocity if the structure were absent at the time of interest,

ν = kinematic viscosity.

Figure 10 shows the coefficient of drag for a smooth cylinder in a steady flow as a function of the Reynolds number, which demonstrates that the coefficient of drag changes dramatically when the flow changes from subcritical to supercritical.

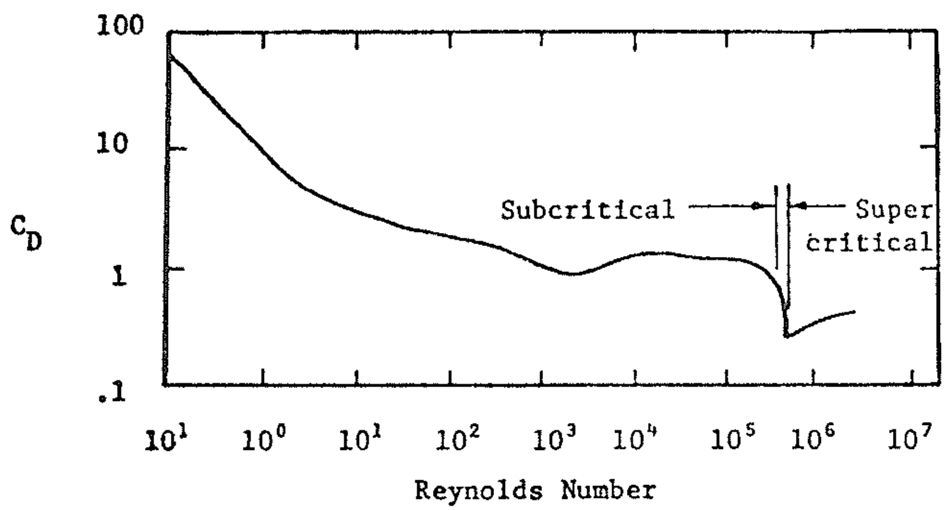

Figure 10 - Drag Coefficient Versus Reynolds Number for a Smooth Circular Cylinder in a Steady Flow

The second parameter, developed by Keulegan and Carpenter, is related to the coefficients of drag and inertia. This dimensionless parameter is also known as the "period parameter," and it relates the maximum amplitude of the oscillating particle velocity including both wave and current (u_{max}) and the period of the oscillatory motion (T) to the diameter of the cylinder (D):

$$N_{KC} = \frac{u_{max}T}{D} \quad \ldots\ldots\ldots\ldots\ldots\ldots\ldots\ldots (14)$$

This parameter has been found to be related to the coefficients of drag and inertia for a very wide range of data.

The coefficients of drag and inertia determined experimentally in this research are presented as functions of these parameters.

Two other major input parameters required by the Morison equation are the particle kinematics of velocity and acceleration.

For a pipeline located near the ocean bottom, the water particle orbits are flattened (parallel to the bottom) for waves where the wavelengths are large compared to the water depth. The orbital motion changes to a horizontally oscillating flow when the water depth is small compared to the wavelength; therefore, in this condition the variation of velocity over the height of the pipe is insignificant. This fact allows the velocity at the midpoint of the cylinder to represent the velocity used in the calculation of the fluid force by the Morison equation.

Several methods have evolved to predict the horizontal velocities under a wave propagating in a current. One simplifying assumption that can be made is to use Airy's[23] linear wave theory. If a uniform current is assumed, the velocity potential of Airy wave theory (ϕ_1) (derived from Laplace equation and linearized boundary conditions) and the velocity potential of the uniform flow field (ϕ_2) can be added directly to obtain the velocity potential (ϕ) of the combined wave-current condition since both potentials are solutions of the Laplace equation.

$$\phi = \phi_1 + \phi_2 \quad \ldots\ldots (15)$$

and

$$\phi_1 = C_o \cosh k_o (Z + d) \sin (k_o x - \omega_o t) \quad \ldots\ldots (16)$$

$$\phi_2 = \bar{U} x$$

where z, d, z, U are defined by Figure 7,

$k_o = \frac{2\pi}{L}$ = wave number for wave in still water,

$\omega_o = \frac{2\pi}{T}$ = frequency for wave in still water,

C_o = celerity for wave in still water.

The horizontal velocity is given by:

$$u = \frac{\partial \phi}{\partial x} = \frac{\partial \phi_1}{\partial x} + \frac{\partial \phi_2}{\partial x} = +C_o k_o \cosh k_o(z+d) \cos (k_o x - \omega_o t) + U \quad \ldots . (17)$$

Rearranging and using the definitions of the wave amplitude and the dispersion relationship, the horizontal velocity u can be written:

$$u = \frac{H}{2} \omega_o \left(\frac{\cosh k_o(z+d)}{\sinh k_o d}\right) \cos (k_o x - \omega_o t) + U \quad \ldots . (18)$$

In a similar manner the horizontal acceleration can be written:

$$\dot{u} = \frac{\partial u}{\partial t} = + \frac{H}{2} \omega_o^2 \left(\frac{\cosh k_o(z + d)}{\sinh k_o d}\right) \sin (k_o x - \omega_o t) \quad \ldots . (19)$$

These equations agree with a basic assumption used in practice: that the velocity field of the wave in still water and the velocity of a current can be summed algebraically to obtain the total velocity field. It should be pointed out that this practice is valid only if the two velocity potentials are solutions to the linear Laplace equation with linear boundary conditions at the surface. This is not the case for steep waves, for which nonlinear boundary conditions are generally applicable resulting in the nonlinear wave theories. Also, if shear currents are present, the superposition principle is not valid. In some cases when steep shallow water waves are present with nonuniform currents, the principle of superposition is still used even though theoretically

it is not valid.

Stokes third order wave theory is also used in conjunction with the current to predict the combined flow field. In this case, the parameters of wave height (H) and period (T) are considered to be the properties of a wave progressing in still water. These parameters are used with the water depth (d) to predict the velocities under a wave if no current were present. These resulting wave velocities are combined algebraically with the current velocity profile to predict the combined velocity profile. The equations and methods to determine the horizontal wave particle velocities were those presented by Skjelbreia[24]. The computer programs used to calculate the particle motion are given in Appendix I for linear and Stokes third-order wave theories.

The effect of the viscous boundary layer of the wave was neglected in the calculation of the horizontal velocity near the bottom. Since the actual current velocity profile was used for superposition, the boundary layer due to the current was taken into account. Therefore any error in the boundary layer was due to neglecting the boundary layer in velocity prediction of the wave theories.

The forces on submerged pipelines are related directly to the velocity field near the structure. The accurate prediction of the horizontal velocity fields is essential for the proper prediction of the forces on submerged pipelines. The error associated with the prediction of the combined horizontal velocity field will be directly related to the error in the calculation of the horizontal force of a submerged pipeline. A knowledge of this error will provide the design engineer an insight into the error associated with the use of the superposition principle for wave-current force calculations.

EXPERIMENTAL APPARATUS AND EQUIPMENT

The experimental study was conducted in a two-dimensional wave-flume facility of the Ocean and Hydraulic Engineering Group at Texas A&M University. The dimensions of the wave flume are 45.72 m (150 ft) in length, 0.46 m (1.5 ft) in width, and 1.22 m (4.0 ft) in depth. The test section was located approximately 18.29 m (60 ft) from the wave generator. Figure 11 shows the general layout of the test facilities.

The wave flume is constructed of a metal and wood frame with one wall consisting of plywood and the other of Plexiglas. Currents are produced by a pumping system capable of developing currents of 1.22 m/sec (4.0 ft/sec). The water depth for any specific flow rate was controlled by an adjustable weir located at the end of the tank.

A wave absorber was constructed to reduce the reflection of the waves. The design permitted large volumes of water to be transmitted through the absorber so that significant currents could be produced. The absorber was constructed of layers of expanded metal and rubberized horse hair material. Gaps of 50.8 mm (2.0 in) were left between the layers of material to allow the fluid to pass through the abosrber at a high rate. The flow-through capacity was further increased by constructing vertical openings midway on the bottom side of the absorber, connecting the interior of the absorber to the flow downstream. These gaps provide flow paths so that the current could pass through the absorber which effectively reduced the reflected waves. A schematic drawing of the absorber is shown in Figure 12, and a photograph of its installation in the flume is

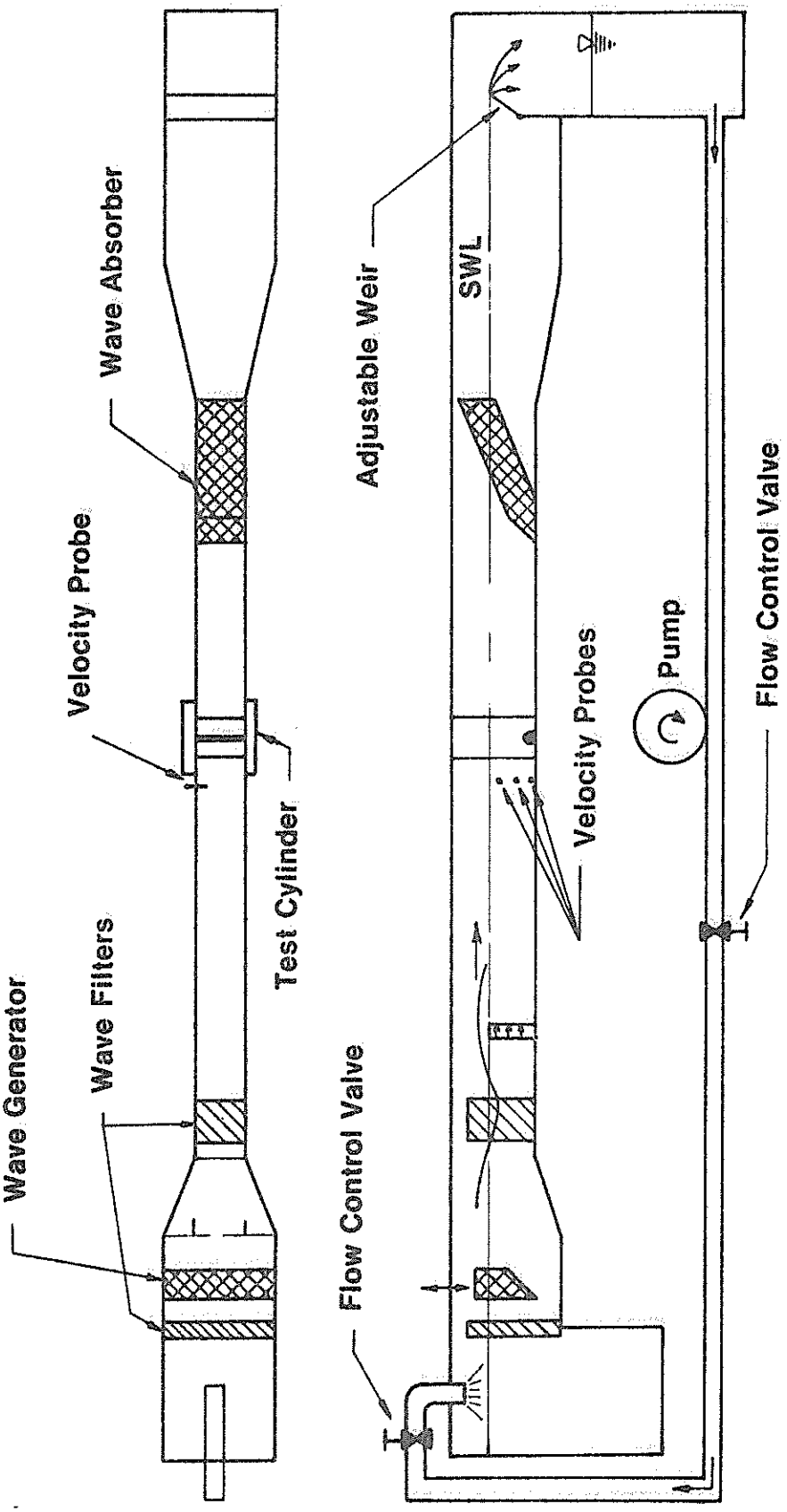

Figure 11 - Wave-Current Test Facility

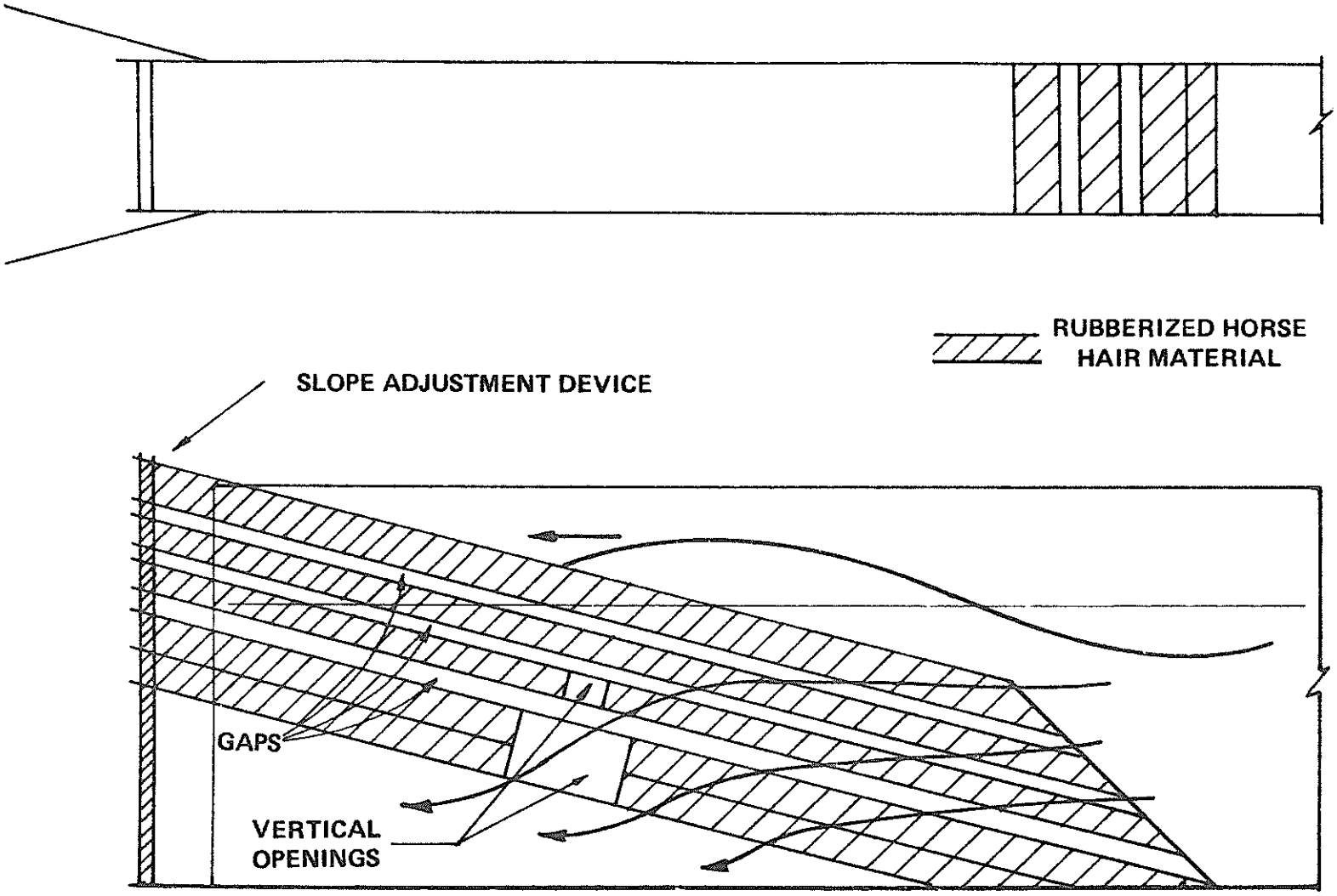

Figure 12 - Schematic Diagram of Current-Passing Wave Absorber

shown in Figure 13. The absorber was found effective for reducing wave reflections for the range of waves used in this research. The maximum reflection coefficient calculated was 12 percent, which was for long, shallow water waves. The absorber was capable of passing currents as high as 0.9144 m/sec (3.0 ft/sec) without significantly reducing the flow of water through the wave flume. The absorber reduced the reflective waves at higher current values, due to the fact that the current swept the reflected energy downstream into the absorber.

A photograph of the wave generator used in this investigation is shown in Figure 14. The generator produces a wave by the plunging motion of a wedge. The generator is driven by a hydraulic system. The speed of the generator is controlled by an electronic valve which controls the flow rate of oil to the hydraulic motor.

The period of generator (and therefore the period of the wave) is adjusted by this valve. The range of periods that could be generated are limited due to the seiching in the wave-basin generating area. The range of periods which could be generated without distortion was 0.8-1.3 seconds. For periods outside this range, the wave produced by the oscillation in the generation area caused secondary waves to be superimposed on the desired wave. The height of the wave was controlled by varying the depth of the plunger. A wide range of wave heights could be generated. The height of the propagated wave was determined by the depth of the plunger and the depth of water.

Filters were used in the locations designated in Figure 11. These filters were constructed of 0.6 cm (0.25 in) wire mesh screen which removed the small surface ripples from the generated waves.

The facilities included two measurement stations as shown in a photograph displayed in Figure 15. Station one was for the measurement

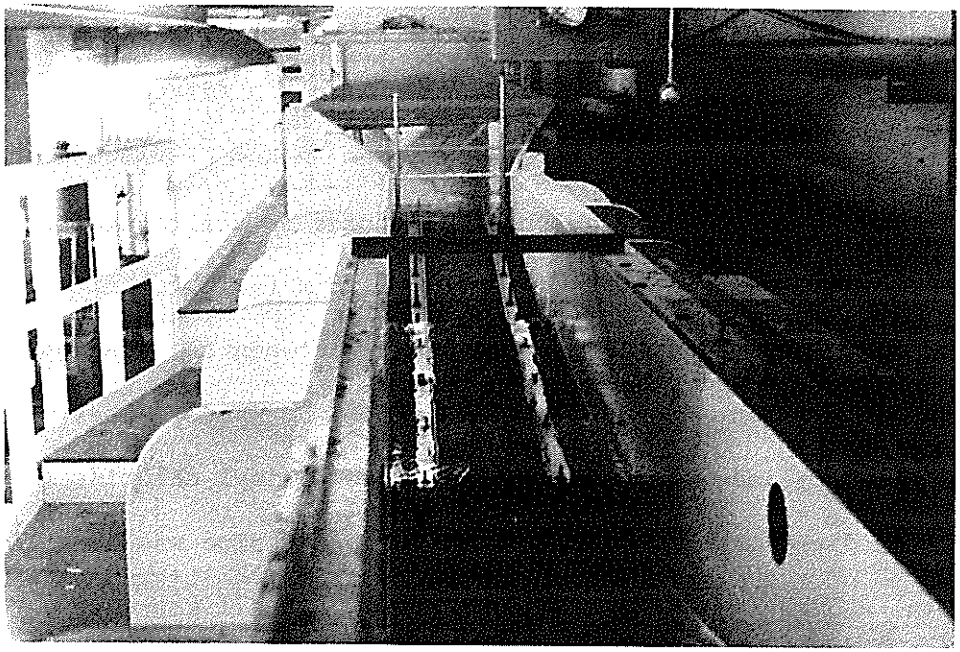

Figure 13 - Current-Passing Wave Absorber

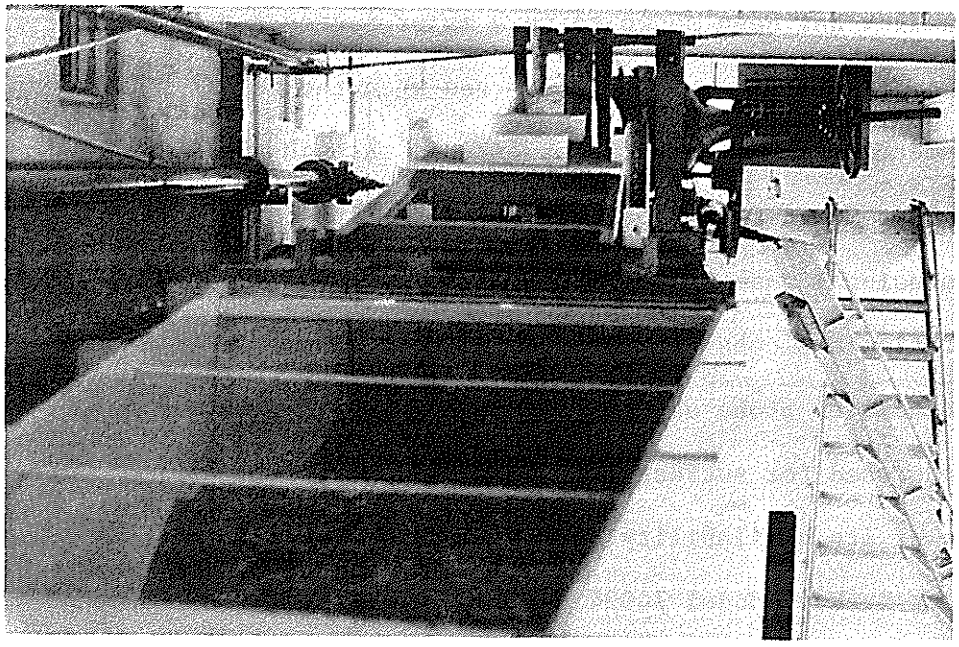

Figure 14 - Wave Generator-Plunger Type

of surface parameters and water particle kinematics; and station two as shown in Figure 16, was for fluid-force determination. Station one was used to gather the information for comparing the predicted water particle to the theoretical values as discussed in the previous section. Station two was used to determine the fluid force on the test structure. Since the distance between the two stations is 1.26 m (4.13 ft), it is assumed that the wave characteristics do not change between the stations. Therefore, the results obtained at station one can be used at station two.

The test cylinder was constructed of poly-vinyl chloride (PVC) pipe. Its outside diameter was 44.5 mm (1.75 in). The pipe was located 1.58 mm (.0625 in) above the bottom of the tank. This small gap was to provide the free movement of the cylinder so that the unrestricted movement is transmitted to the load cell which converts this movement to an applied force. Since only horizontal components of force were being measured the effect of the gap is minimized. The spacing of the cylinder from the boundary has been shown to be a major factor for vertical forces but is insignificant for horizontal forces when the gap is small compared to the diameter. The test cylinder extends through the walls of the test tank. This extension helps to reduce end effects, which supports the two-dimensional assumption.

Station one consisted of a capacitance-type wave gauge and a hot-film anemometer probe as shown in Figure 17. The capacitance-type wave gauge was used for surface profile measurements of wave height and period because of its availability and linearity. The results were recorded on a Hewlett Packard Model 74024 oscillographic strip recorder. This recorder is capable of providing a time reference on the recorded data. The period of the wave was determined by measuring the time between two successive wave crests. The capacitance-type wave gauge was used with

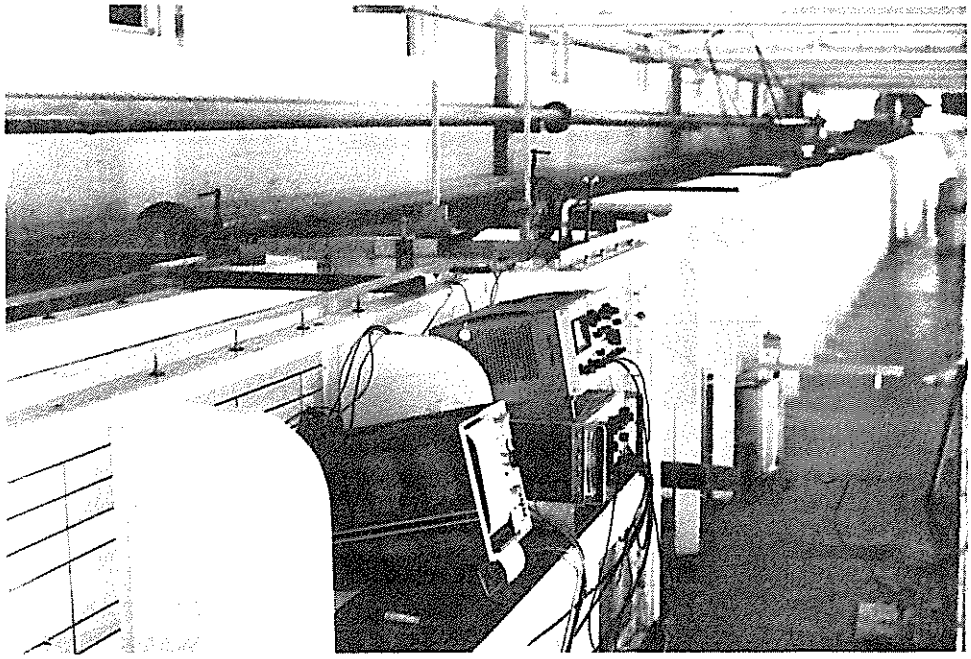

Figure 15 - Experimental Stations One and Two

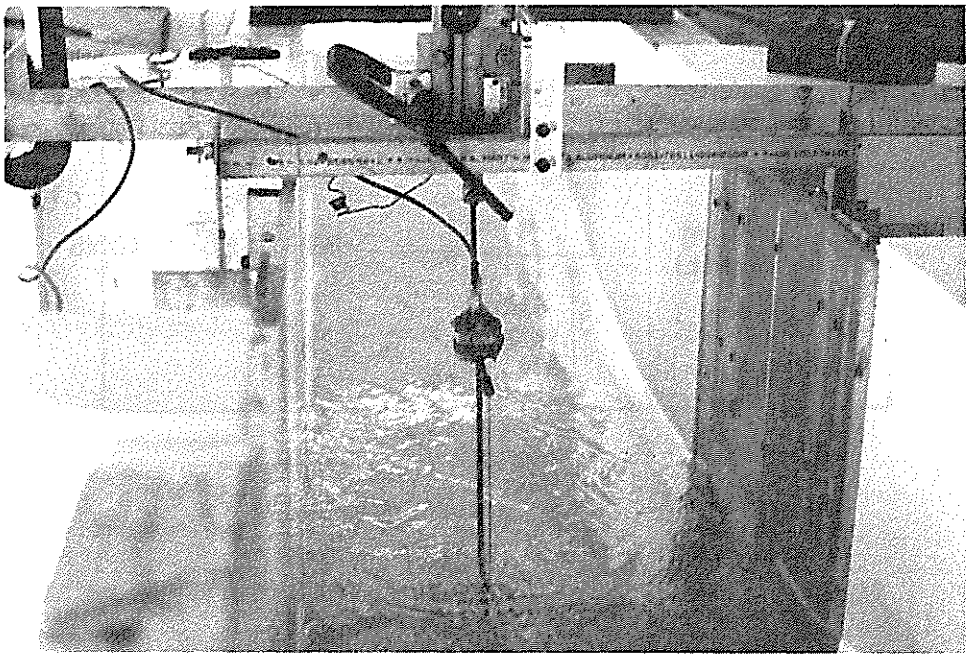

Figure 16 - Experimental Station Two. Wave Force Determination

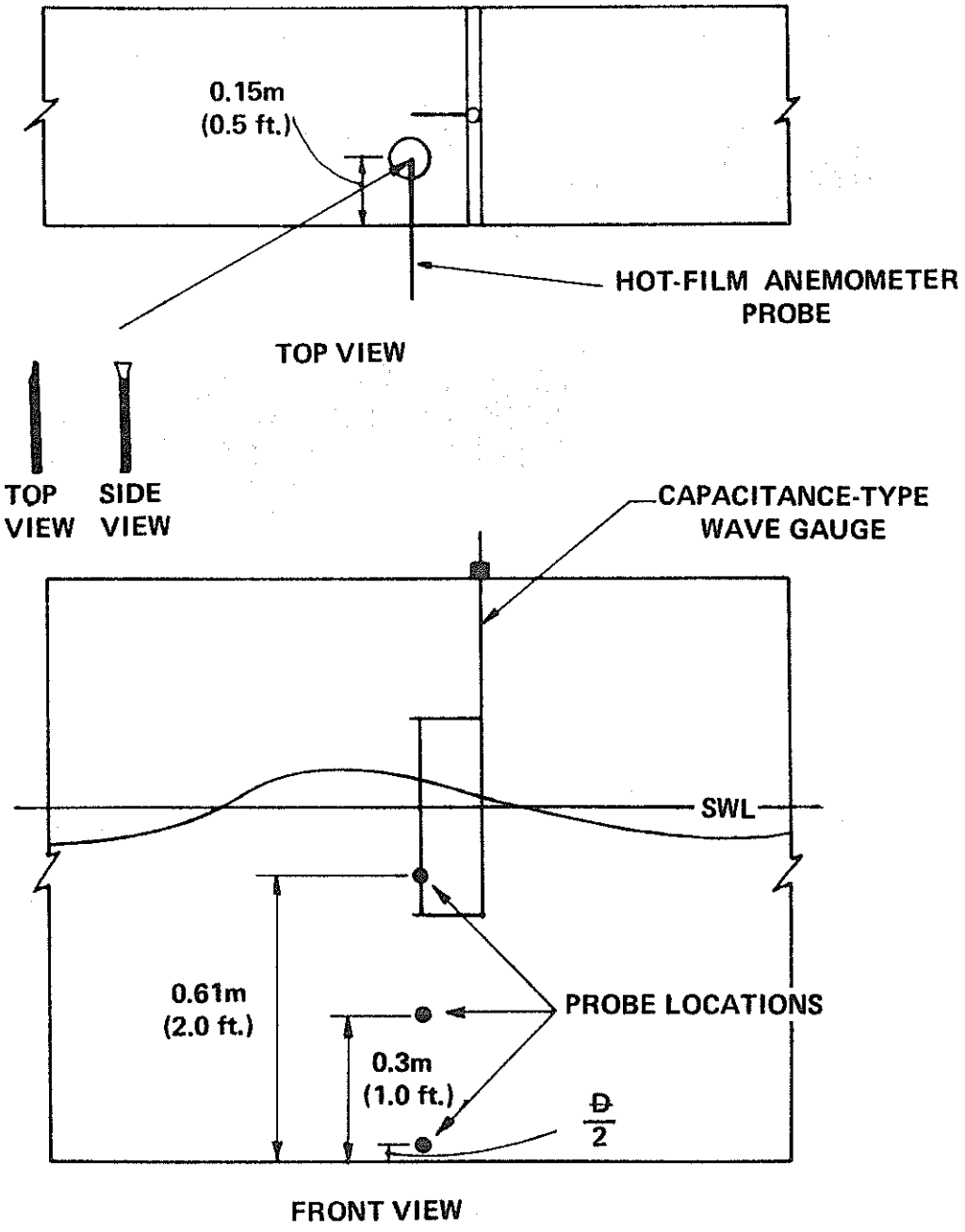

Figure 17 - Experimental Station One. Surface Profile and Velocity Measurements

a Hewlett Packard Model 17403A Carrier preamplifier. This preamplifier contained the full-bridge network required by the capacitance-type wave gauge. The output of the hot-film anemometer was amplified by a Hewlett Packard Model 17402A Low-Gain preamplifier before the output was recorded on a strip recorder.

A Thermo-Systems Model Series 1050 hot-film anemometer was used for the particle velocity measurements. This series consisted of a Model 1050A constant-temperature anemometer, a Model 1051 monitor and power supply, a Model 1055 linearizer, and a Model 1057 signal conditioner.

The transducer used with the anemometer is a small resistance element which is heated and controlled at an elevated temperature. A Model 1210-20 hot-film transducer (probe) was used in this research. The amount of electrical energy dissipated in the sensor is a measure of the cooling effect of the fluid flowing past the heated sensor. The cooling effect of the fluid passing over the sensor depends on both the mass flow and temperature difference between the sensor and the fluid. The relationship between bridge voltage and mass flow or mass flux is as follows:

$$\frac{E^2 R}{(R+R_3)^2} = A + B\,(\rho v)^{\frac{1}{n}}\,(t_s - t_e) \quad \ldots\ldots\ldots\ldots\ldots\ldots\ldots\ldots (20)$$

where

A,B = constants depending on fluid and type of sensor

ρ = density of fluid

v = velocity

n = exponent (close to 2)

t_s = sensor operating temperature

t_2 = fluid or environmental temperature

$t_s - t_e$ = typically 40°C in water

R = sensor operating resistance

R_3 = resistor in series with sensor (usually 40 ohms)

E = bridge voltage

In operation, a current flows through the bridge. The amplifier senses any off balance, and feeds back more or less current until the bridge comes into balance. This additional electrical energy is outputted as a bridge voltage which is amplified and recorded on the oscillographic strip recorder. It can be seen from equation (20) that this output voltage is related to the velocity by a highly nonlinear relationship. The following section describes the methods used to calibrate this device in oscillating flows.

It can be seen from Figure 17 that three locations were used for water particle measurements. They were at 0.61 m (2.0 ft), 0.31 m (1.0 ft) and at the mid height of the cylinder at the bottom of the tank. The particle kinematics were compared at these elevations. The particle velocity at the mid height of the cylinder was used with the measured fluid force to determine the coefficient of drag. The probe was extended into one side of the tank a distance of 0.15 m (0.5 ft). This distance was selected so that the measured particle velocity would be out of the boundary layer, but the distance was short enough to reduce the effect of probe vibrations due to vortex shedding. The orientation of the probe in the fluid flow is important, because by aligning the probe perpendicular to the flow, only the horizontal component of the velocity is measured. The velocity parallel to the probe is not significant and can be assumed to be zero. With the orientation shown in Figure 19, only the horizontal velocity component was recorded. Only horizontal velocities and forces

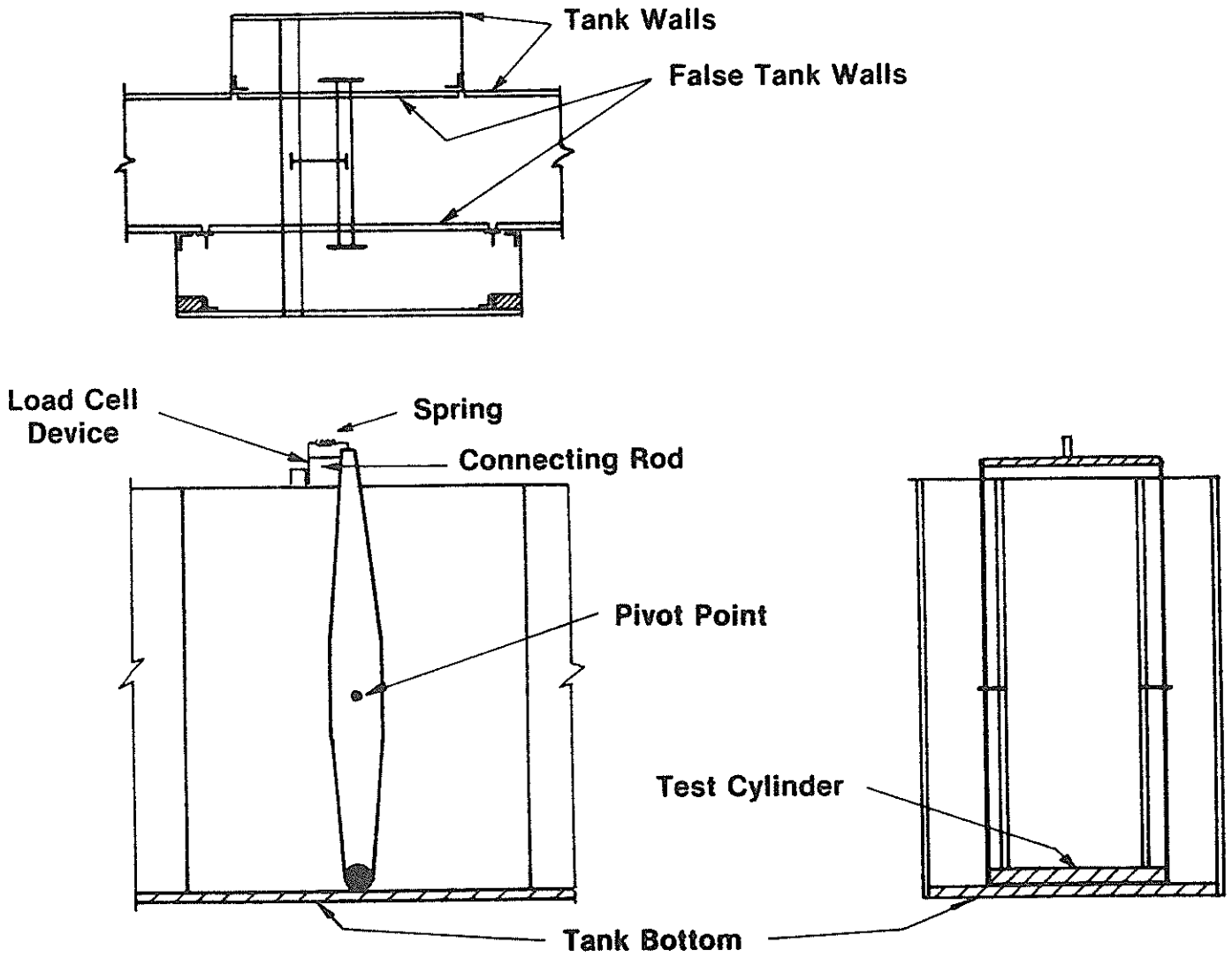

Figure 18 - Schematic Diagram of Station Two, Model Load Test Station

were investigated in this research.

Station two consisted of a capacitance-type wave gauge and a mechanism to transmit the horizontal forces on a horizontal circular cylinder resting near the bottom to a load-cell device. A schematic of station two is shown in Figure 18. The cylinder was connected by two arms which rotated about a pivot point. This rotation transmitted the horizontal fluid force on the cylinder to a load cell located on the top of the tank. The load cell has a capacity of 1500 grams (≈3.0 lbs). The load cell was connected to the rotating mechanism by a rod which was pointed on both ends and which is held in place by a stiff spring. These pin-point connections were used to reduce friction. This total mechanism was capable of transmitting the positive or negative fluid force to the load cell without disrupting the fluid flow near the model. The device was balanced around the pivot points, so that any inertial force of the mechanism would pass through the pivot points. This device was found to be very effective in measuring the fluid force on the horizontal cylinder.

CALIBRATION AND PROCEDURE

All the equipment used in this investigation was calibrated using known values which were related to the output on the oscillography recorder. All equipment was re-calibrated at each major test except for the hot-film anemometer which had to be calibrated periodically during the testing due to drift of the output.

The capacitance-type wave gauge was calibrated in calm water before the testing began. The device was connected to the carrier preamplifier which contained the bridge network required for the device. The gauge was balanced by the recommended procedure of Hewlett Packard. The balancing consisted of adjusting the internal resistance and capacitance of the bridge in order to balance the resistance and capacitance of the gauge and connecting cables. This procedure assured that any change in the capacitance across the bridge was due to the change in the elevation of water detected by the capacitance network of the gauge. Once the balancing procedure was complete, known changes in the water elevation were applied to the gauge and the resulting movement of needle on the recorder was noted. These changes were accomplished by moving the gauge a known distance 30.5 mm (0.1 ft) typically in the water. From the number of divisions that the output changed for each increment of depth at the gauge, a ratio was calculated that related the change in elevation of the water to the number of divisions recorded. This ratio was used to determine the elevation of the water surface as a function of time. The ratio was computed at all increments so that the linearity of the

gauge was confirmed. The gauge proved to be linear throughout the actual testing period of the research.

The load cell was calibrated and balanced in a manner similar to the capacitance-type wave gauge. A known load was applied to the test cylinder, and the output of the bridge network was recorded on the oscillograph recorder display. The applied load was transferred through a system of pulleys and weights described by the schematic diagram shown in Figure 19. The total force applied to the cylinder is equal to the suspended weight multiplied by the length ratio of the arms around the pivot point. Any losses due to friction were neglected. The known load is related to the output voltage recorded on the oscillography display by a linear ratio. A sample output of the oscillograph recorder for the known loads is shown in Figure 20. This output shows that the load cell device was linear, and the ratio was calculated with an error range of plus or minus 6%. Additional calibration tests were conducted for larger applied loads in both directions. These tests supported the fact that the load to a maximum of 500 grams (1.102 lbs) in either direction was represented by a linear ratio. Figure 20 shows that as the load was released, the bridge output voltage returned to zero. This indicates that at zero applied load, the recorder returns to the zero output voltage, and the load cell is well within its linear range.

Calibration of the hot-film anemometer proved to be difficult, due to its nonlinear output and the constant drift of the output voltage. The hot-film anemometer was calibrated by means of known velocities created by a forced pendulum. A schematic of the forced pendulum is shown in Figure 21. The angular velocity (ω_1) of the driving mechanism is related to the velocity of the probe by the following equation:

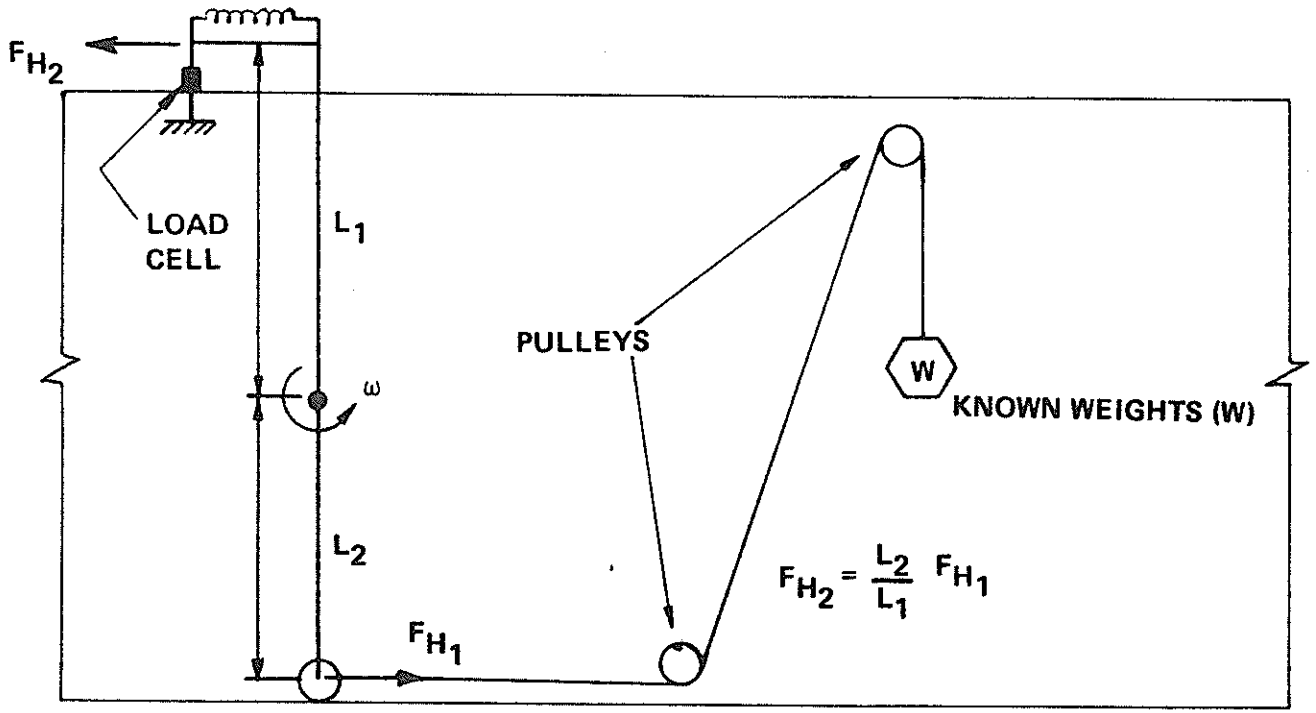

Figure 19 - Schematic Diagram of Load-Cell Calibration Apparatus

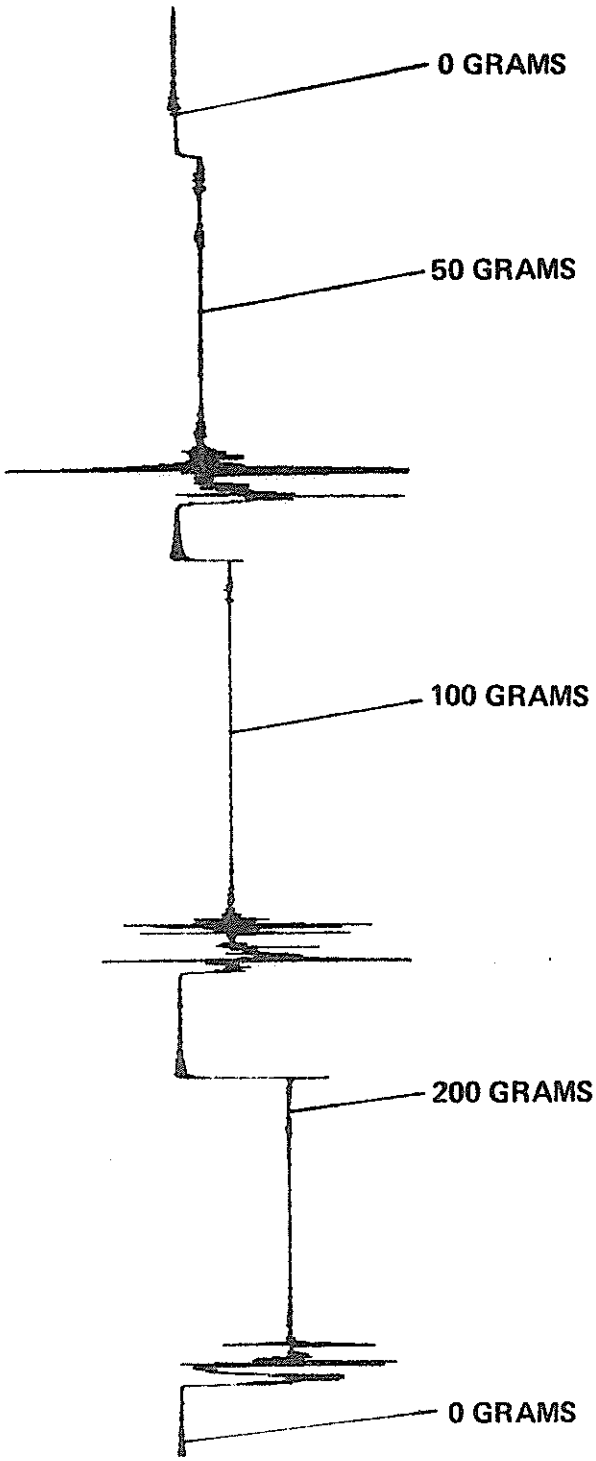

Figure 20 - Output for Load-Cell Calibration

V_p = velocity of probe (ft/sec) = .7857 (ω_1) . . . . . .(21)

V_p = velocity of probe (m/sec) = 0.2395 (ω_1) . . . . . .(22)

Four angular velocities were used to calibrate the probe. The angular velocities and the related velocities are listed in Table 2.

Table 2 - Velocity calibration points

Calibration Point	Angular Velocity (ω) rad/sec	Velocity of Probe (V_p) m/sec	ft/sec
1	4.7306	1.1328	3.7166
2	1.8938	0.4535	1.4879
3	0.9492	0.2273	0.7457
4	0.4728	0.1132	0.3715

These four known velocities are used as calibration points for the hot-film anemometer. These velocities were measured using the same apparatus as the wave particle kinematics. The number of divisions for each calibration point was related to the velocity by fitting the data to a power curve. A sample of the output of a calibration test is shown in Figure 22. The graph showing the calibration points and the computed curve of the curve fitting process is shown in Figure 23. This figure shows that there is agreement between the calibration data and power curve fit.

An inherent problem of the hot-film anemometer is that the calibration will drift in a relatively short period of time. It was determined that significant drift occurred in a period of several hours. To overcome this problem, the drift as a function of time was investigated. It was determined by running successive calibration tests during a period of one hour. Figure 24 shows the calibration drift of each calibration

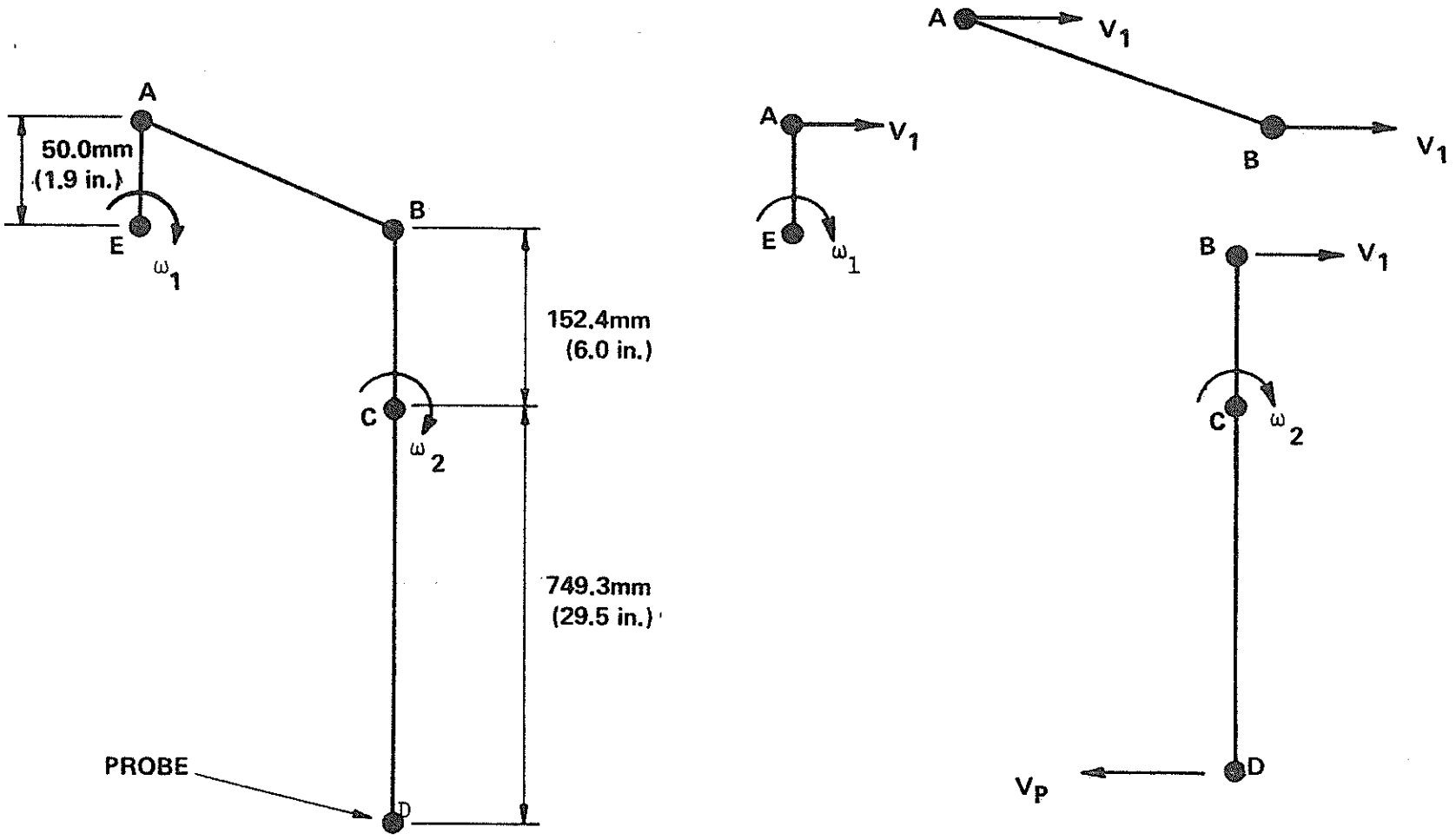

Figure 21 - Schematic Diagram of the Forced Pendulum for Velocity Calibration

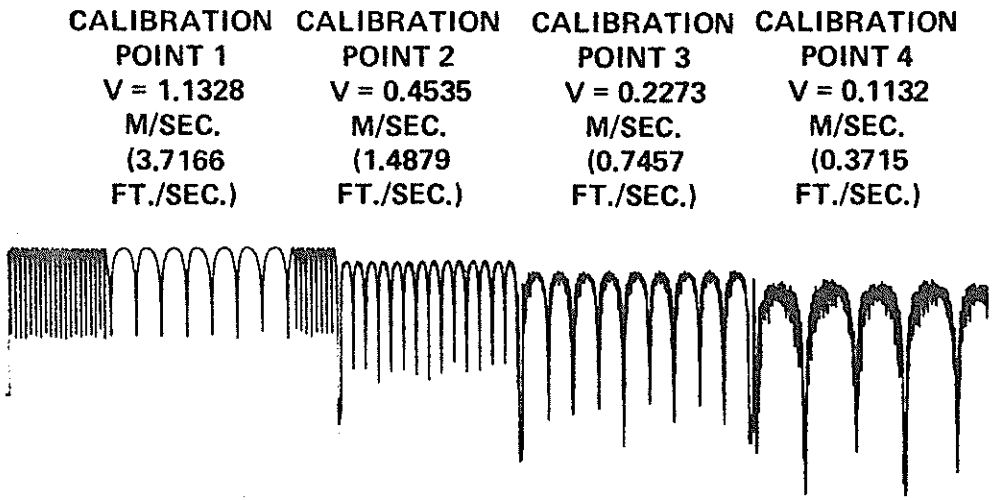

Figure 22 - Sample Calibration Output for Hot-Film Anemometer

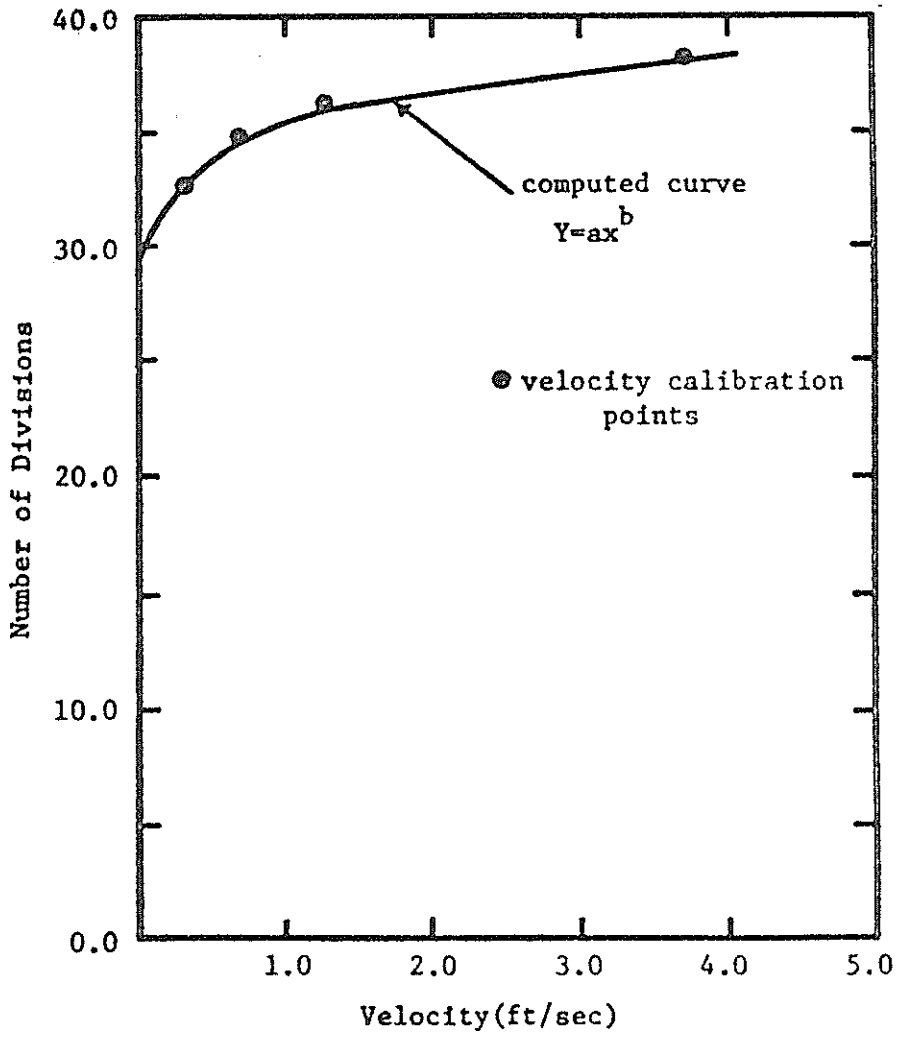

Figure 23 - Calibration Curve for Hot-Film Anemometer

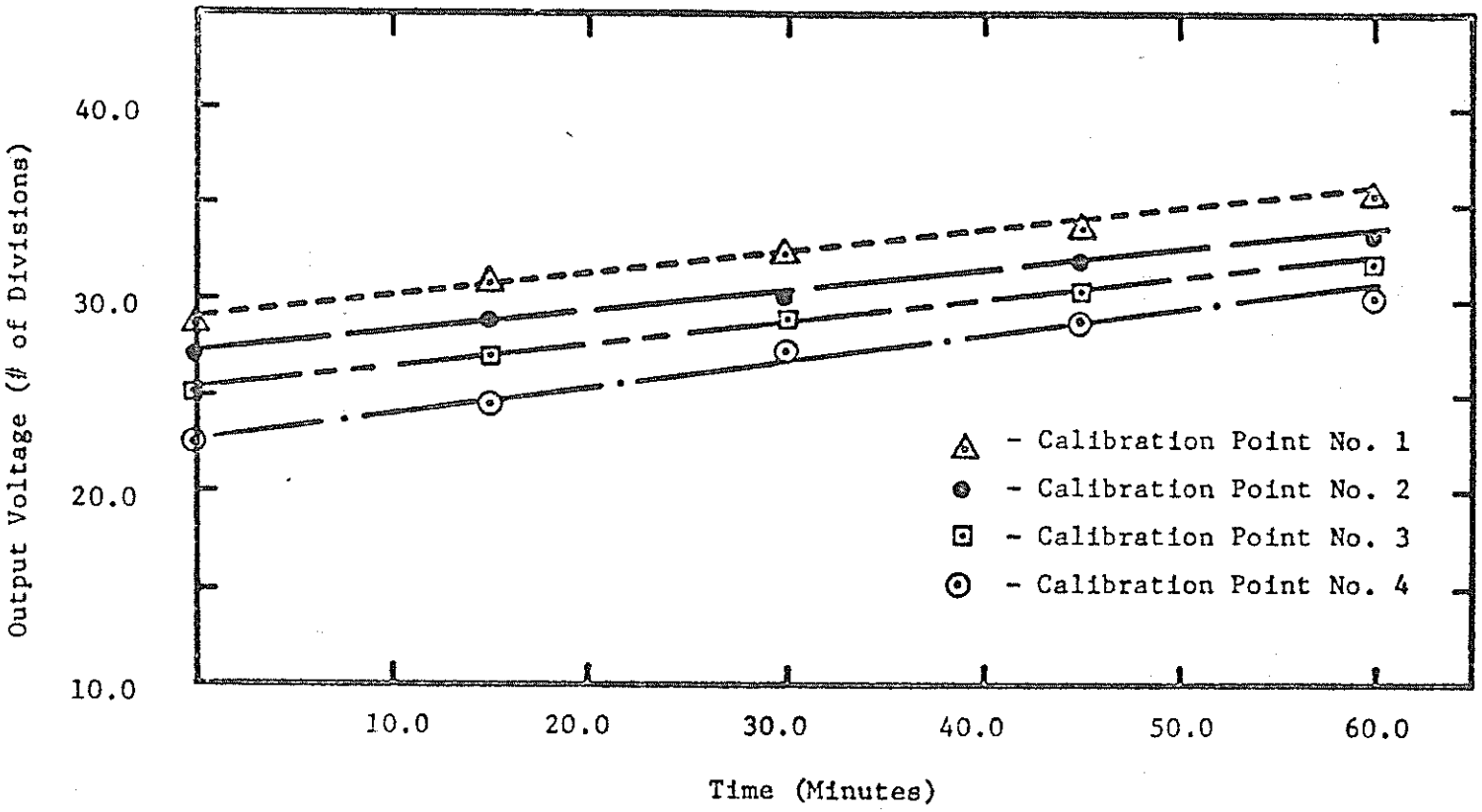

Figure 24 - Calibration Drift of Hot-Film Anemometer

point at four intervals of 15 minutes. The drift during the hour period was reasonable linear. Calibration tests were run periodically during the test periods. Graphs similar to Figure 24 were constructed and the calibration points for the curve-fitting program were determined from the graph at the time the individual test was conducted. This procedure proved successful for calibrating the hot-film anemometer.

The velocity measured by the procedure outlined above was checked against an electromagnetic current meter. Even though the electromagnetic current meter was a much coarser velocity measurement device, the values measured by both devices agreed reasonably well. The comparison of the two devices is summarized in Table 3.

Table 3 - Comparison of velocities of electromagnetic current meter and hot-film anemometer

Electromagnetic Current Meter		Hot-Film Anemometer	
m/sec	(ft/sec)	m/sec	(ft/sec)
0.0000	(0.00)	0.0000	(.0000)
0.0366	(0.12)	0.0151	(.0497)
0.0640	(0.21)	0.0618	(.2027)
0.1219	(0.40)	0.1432	(.4698)
0.1829	(0.60)	0.1751	(.5745)
0.2438	(0.80)	0.2352	(.7717)

The testing program was divided into two major stages. One stage was the determination of the water particle kinematics at three elevations with the wave surface parameters; the other was the measurement of the simultaneous fluid-force measurements and particle kinematics measurements required to determine the coefficient of drag.

The procedure for stage one began with the calibration of the capacitance-type wave gauge and the hot-film anemometer in still water. The wave flume was then drained, so that the probe of the hot-film anemometer could be removed from the calibration apparatus and inserted in the wave flume. The probe and probe holder had to be moved as a unit so that the calibration would not change. For the first set of tests, the probe was inserted at an elevation of 0.61 m (2.0 ft) above the flume bottom. The wave flume was then refilled to the desired water depth. Tests were conducted in still water over a range of water depths with varying wave heights and periods. The time at which each measurement was taken was noted. These times were used to determine the calibration data for the hot-film anemometer as discussed previously. Currents of varying magnitude were then produced in the wave flume. Tests were conducted at each current velocity for a range of waves and water depths. This process was continued for other current velocities. Re-calibration of the anemometer was conducted at hourly intervals. At these times the flume was drained, the probe and probe holder were removed and connected to the calibration device, and the calibration test was conducted noting the time. The flume was again drained, and the probe was switched again to the flume. This process was continued until the required data cases were completed.

All data were recorded on the oscillograph recorder and digitized and then used as input for a computer program which fitted the velocity data to a power curve. This program then wrote the calibrated data and other parameters of the particular test to a computer data file, where it was stored for computer analysis.

The above procedure was repeated for a particle velocity measurement at an elevation of 0.3048 m (1.0 ft) above the bottom.

The second stage was completed in a similar manner to that of stage one, the difference being that simultaneous force data were taken. The velocity used to determine the coefficient of drag was measured at an elevation of half the pipe diameter above the bottom.

For each particular wave test, the data at the velocity measurement station were related to the force measurement by the wave surface parameters, although the data for each station was recorded on separate oscillograph recorders. It was assumed that the velocity under the crest determined at station one was the velocity that would be experienced at the test cylinder under the crest. The velocities were digitized in conjunction with the force measured at the crest, trough, and upcrossings. All measurements were stored on data files by a computer program which performed the necessary calibration.

The data were analyzed by a Interdata 5-16 micro-computer located at the Hydrodynamics Laboratories at Texas A&M University. The computer programs used to perform the calibration and data analysis are given in Reference 26.

DATA ANALYSIS AND RESULTS

The results obtained from the testing program are based on several assumptions. First, the wave reflections from the sides and end of the wave tank are considered to have very little effect on the measurements. Secondly, the flow was assumed to be essentially two-dimensional. This is supported by the fact that the aspect ratio of the model was 10.274. Thirdly, the flow was considered irrotational, and the fluid was inviscid. This assumption, which is vital for the validity of the superposition principle, has been found to be incorrect for currents with a varying velocity profile. The quantification of the error associated with this assumption was the basic goal of the research.

The thrust of the data analysis was two-fold. One task was to determine the error associated with the superposition of the current velocity field and the velocity field generated by a wave propagating in still water. This was accomplished by directly measuring the error over a specific range of waves and currents. The velocity field of the waves was predicted by both Airy and Stokes third order wave theories.

The other task was a comparison of the measured forces on the pipeline model with the forces predicted by this superposition principle. The experimental drag coefficients were determined by the simultaneous measurement of horizontal fluid velocity and fluid force. Comparisons were then made to the coefficients determined from the superposition principle using Airy or Stokes third order wave theories.

For the first task, kinematic measurements were taken at three elevations

as discussed previously. The second task employed a fourth test to measure forces on the model pipeline. The range of wave parameters and currents tested are presented non-dimensionally in Table 4. Since tests 3 and 4 were conducted simultaneously, the range of values for both tests was identical.

The raw data for tests 1-3 consisted of wave heights, wave periods, and a continuous measurement of horizontal fluid velocity over the wave period. The raw data for test 4 included a continuous record of horizontal fluid force over the period. The estimated error associated with each of these input variables is presented in Table 5. The largest error was associated with the fluid velocity measurements of the hot-film anemometer. The error reached its maximum at the lower velocities, which were not within the range of the calibration curves.

The continuous force and velocity recordings over each wave period were digitized at four equally spaced points. These four points and the corresponding phase angles in the Eulerian reference frame are presented in Table 6.

Data points 1 and 3 correspond to the wave crest and trough, respectively, and data points 2 and 4 correspond to the upcrossings for Airy wave theory (and are near the upcrossings for Stokes third order wave theory). These four points were chosen because of their importance in determining the fluid force on the test cylinder. The maximum positive and negative drag forces (f_d) correspond to the data points one and three, respectively. The maximum acceleration occurs at the upcrossings, which correspond to data points 2 and 4.

The relative error of the superposition principle of the horizontal velocities can be expressed as a dimensionless difference (E):

Table 4 - Ranges of Wave and Current Parameters for Testing Program

Test	$\frac{H}{d}$	$\frac{H}{gT^2}$	$\frac{d}{gT^2}$	$\frac{U}{u}$	$\frac{H}{L}$
1. Horizontal Particle Velocity Measurement at Elevation 0.61 m (2.0 ft)	0.1358-0.291803	0.0415-0.0230	0.0639-0.1102	0.1439-1.0179	.09896-.09186
2. Horizontal Particle Velocity Measurement at Elevation 0.30 m (1.0 ft)	0.1715-0.2912	0.0107-0.0238	0.0551-0.1253	0.0000-5.3316	.07265-.12429
3. Horizontal Particle Velocity Measurement at Elevation 0.02 m (0.146 ft)	0.1155-0.2407	0.0128-0.0197	0.0563-0.1155	0.0000-4.9602	.08699-.12508
4. Horizontal Force Measurement	0.1155-0.2407	0.0128-0.0197	0.563-0.1155	0.0000-4.9602	.08699-.12508

Table 5 - Estimated Accuracy of Experimental Measurements

Variable	Maximum Error	Major Source of Error
Wave Height	2 to 5 percent	Stability and linearity of bridge network and recording device; wave reflection.
Wave Period	±.05 seconds	Determination of wave crest from recording device.
Water Depth	6 mm (.25 in.)	Varying water depth due to current.
Fluid Force	2 to 3 percent	Determination from recorded output; stability and linearity of bridge network.
Fluid Velocity	1 to 8 percent	Calibration and drift of hot-film anemometer (This error is greatest at low velocity due to curve fit process of output voltage to velocity).

Table 6 - Definitions of raw data points for continuous force and velocity records.

Data Point	$\frac{t}{T}$	$\theta = -w_o t = \frac{-2\pi t}{T}$
1	0.0	0.0
2	0.25	-1.5708
3	0.50	-3.1416
4	0.75	-4.7124

$$E = \frac{u_{mea} - u_{tot}}{\frac{\pi H}{T}} \quad \ldots\ldots\ldots\ldots\ldots\ldots\ldots\ldots\ldots\ldots\ldots\ldots (23)$$

where u_{mea} = the measured horizontal velocity at elevation (z),

u_{tot} = algebraic sum of the horizontal particle velocity at elevation (z) predicted by either Airy or Stokes third order wave theory and the current velocity,

H,T are defined previously.

The difference was non-dimensionalized by dividing by the Airy deepwater horizontal velocity at the still water elevation.

The dimensionless difference (E) was found to be a function of a dimensionless parameter (R) relating the magnitude of current to the horizontal particle velocity of the wave in still water:

$$R = \frac{U}{u_{calc}} \quad \ldots\ldots\ldots\ldots\ldots\ldots\ldots\ldots\ldots\ldots\ldots\ldots (24)$$

where U = current velocity at elevation (z)

u_{calc} = horizontal particle velocity predicted by either Airy or Stokes third order wave theories in the absence of a current at elevation (z).

The relationship between the dimensionless difference (E) and the velocity ratio (R) for the three elevations at data point one are shown in Figures 25-27 for Airy wave theory and in Figures 28-30 for Stokes third order wave theory. Similar plots for data point three are shown in Figures 31-33 for Airy wave theory and in Figures 34-36 for Stokes third order wave theory.

Several interesting results can be noted from these figures. The wave theories tend to under predict (positive dimensionless difference for data point one; negative dimensionless difference for data point three) the horizontal velocity at elevation (z) when no current is present (R = 0.0). As the current velocity increased relative to the wave particle velocity, the error decreased to approximately zero to R > 1.0. This trend is represented by the dotted lines on each of the figures. This trend seems to indicate that the superposition of the velocity fields approaches reasonable agreement with the measured values for R > 1.0.

The most extensive tests were conducted at the 0.30 m (1.0 ft) elevation which had the best correlation to this trend. Fewer tests were conducted at the other elevations. The correlation was poor at the 0.61 m (2.0 ft) elevation, because significant error was introduced when the probe was exposed to the air at the troughs of the larger waves, causing extensive calibration drift.

The figures also suggest that the velocity error at the elevation of 0.02 m (0.073 ft) does not approach zero as fast as the velocities at the higher elevations. This additional error must be primarily due to inadequacies in the wave theories, since the actual current velocities at this elevation were used for superposition.

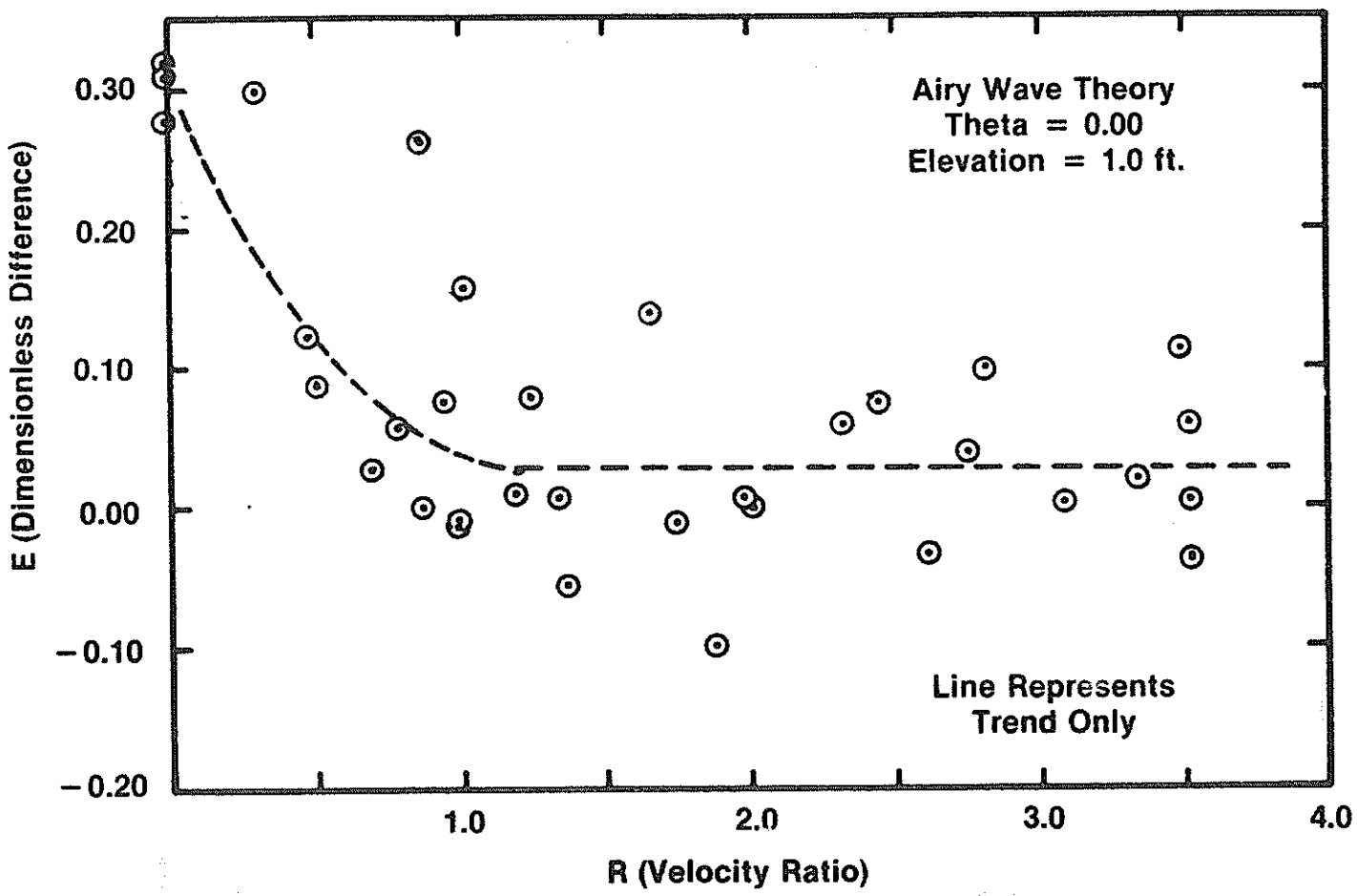

Figure 25 - Dimensionless Difference Versus the Velocity Ratio for Airy Wave Theory at Elevation 1.00 ft (Theta=0.00)

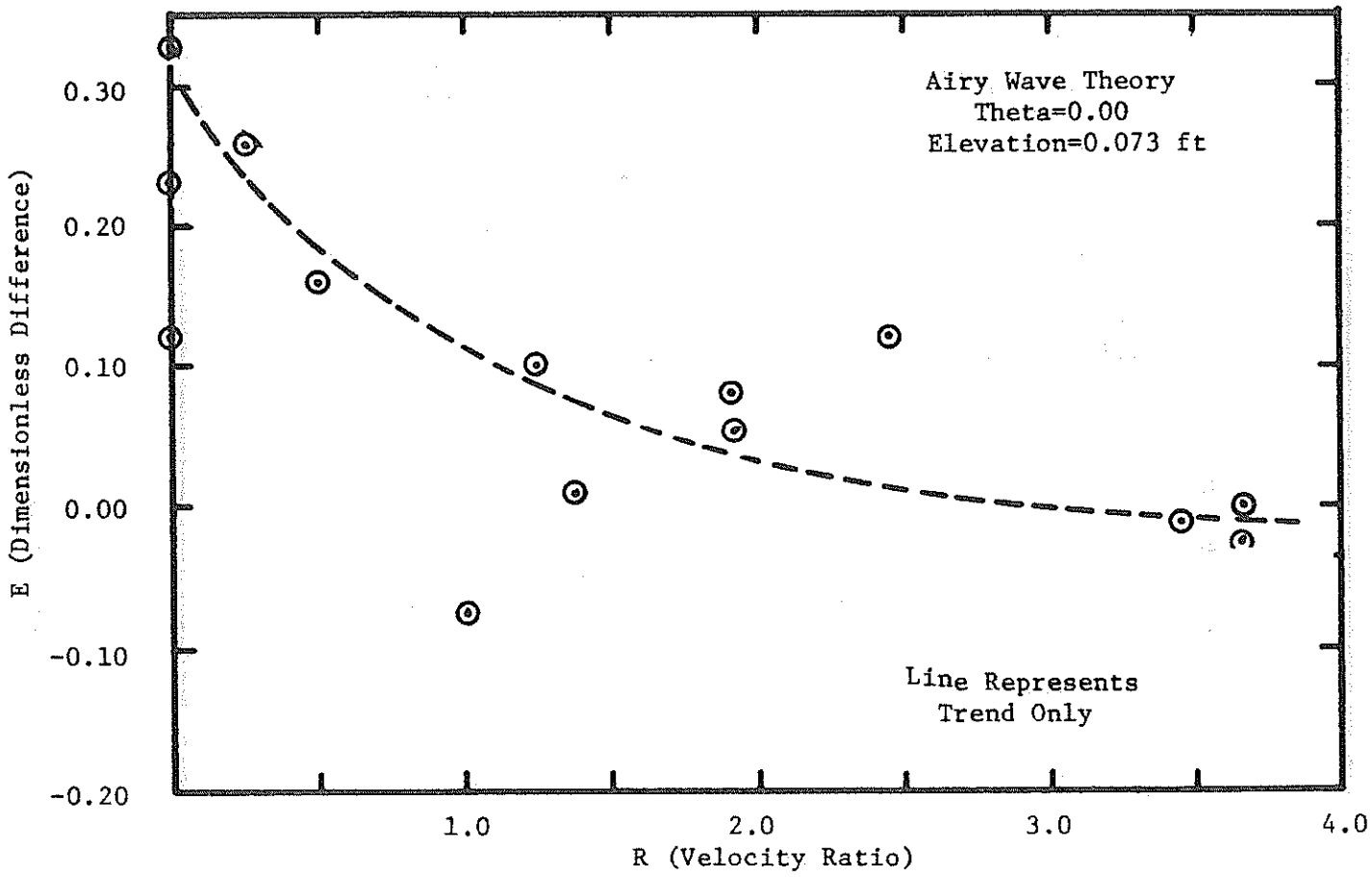

Figure 26 - Dimensionless Difference Versus the Velocity Ratio for Airy Wave Theory at Elevation 0.073 ft (Theta=0.00)

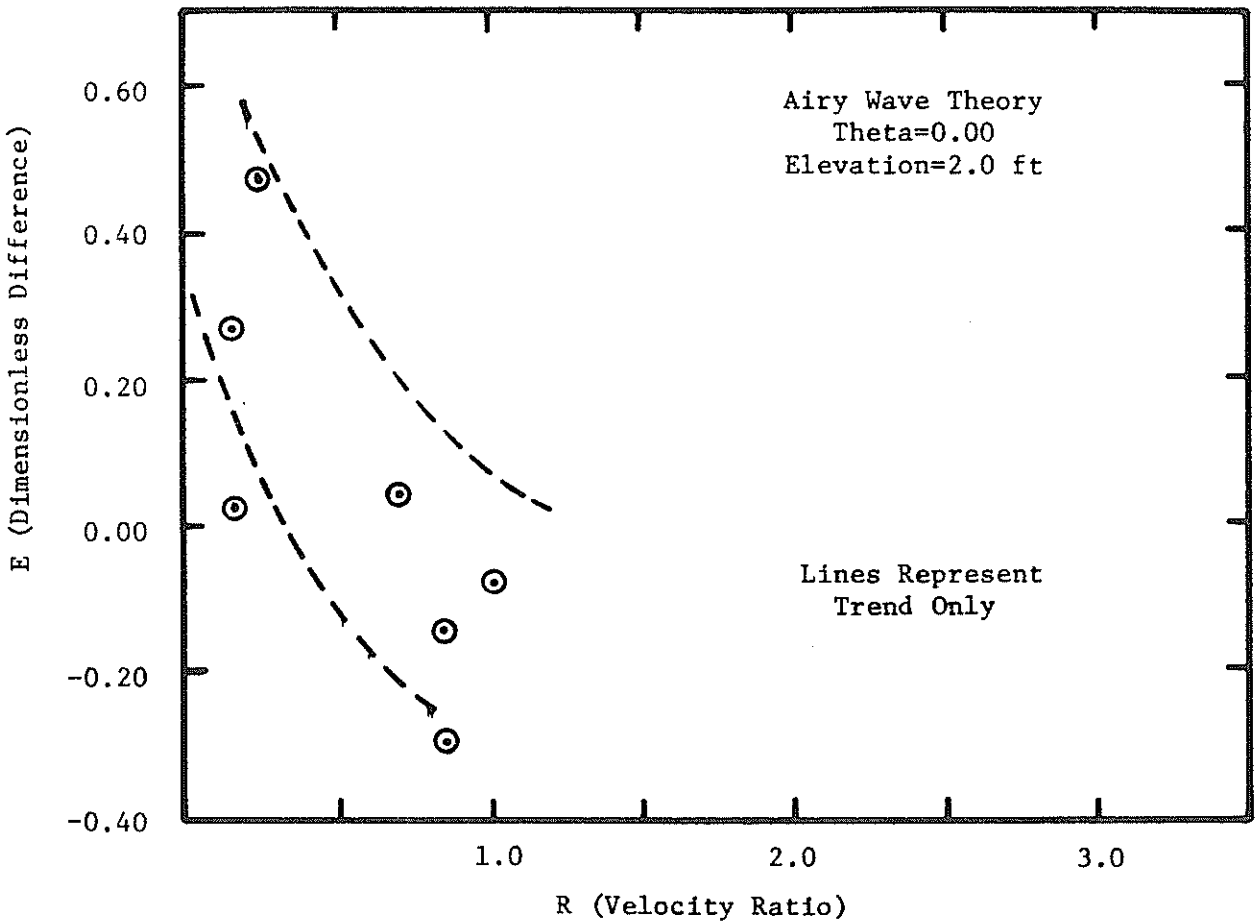

Figure 27 - Dimensionless Difference Versus the Velocity Ratio for Airy Wave Theory at Elevation 2.00 ft (Theta=0.00)

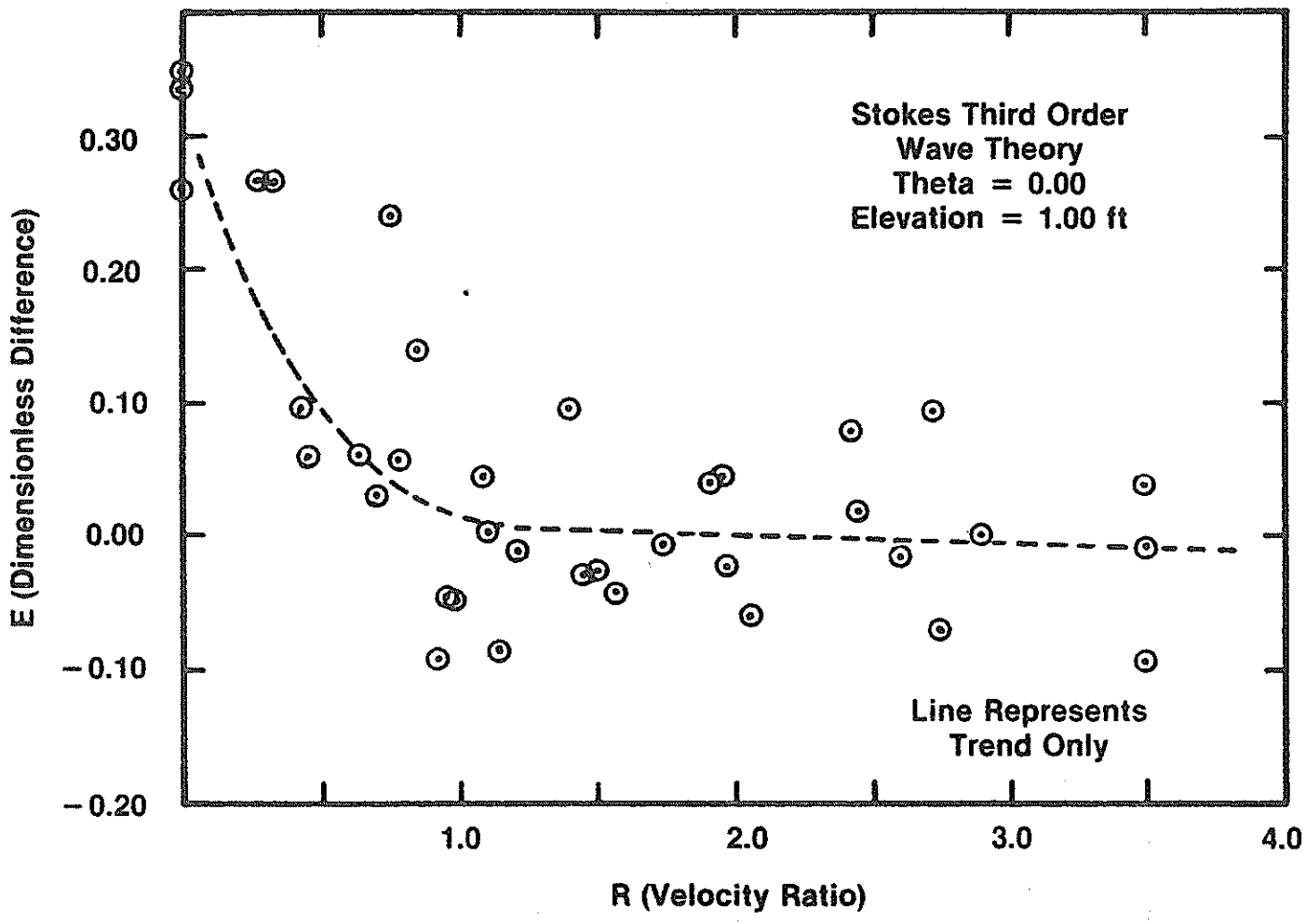

Figure 28 - Dimensionless Difference Versus Velocity Ratio for Stokes Third Order Wave Theory at Elevation 1.00 ft (Theta=0.00)

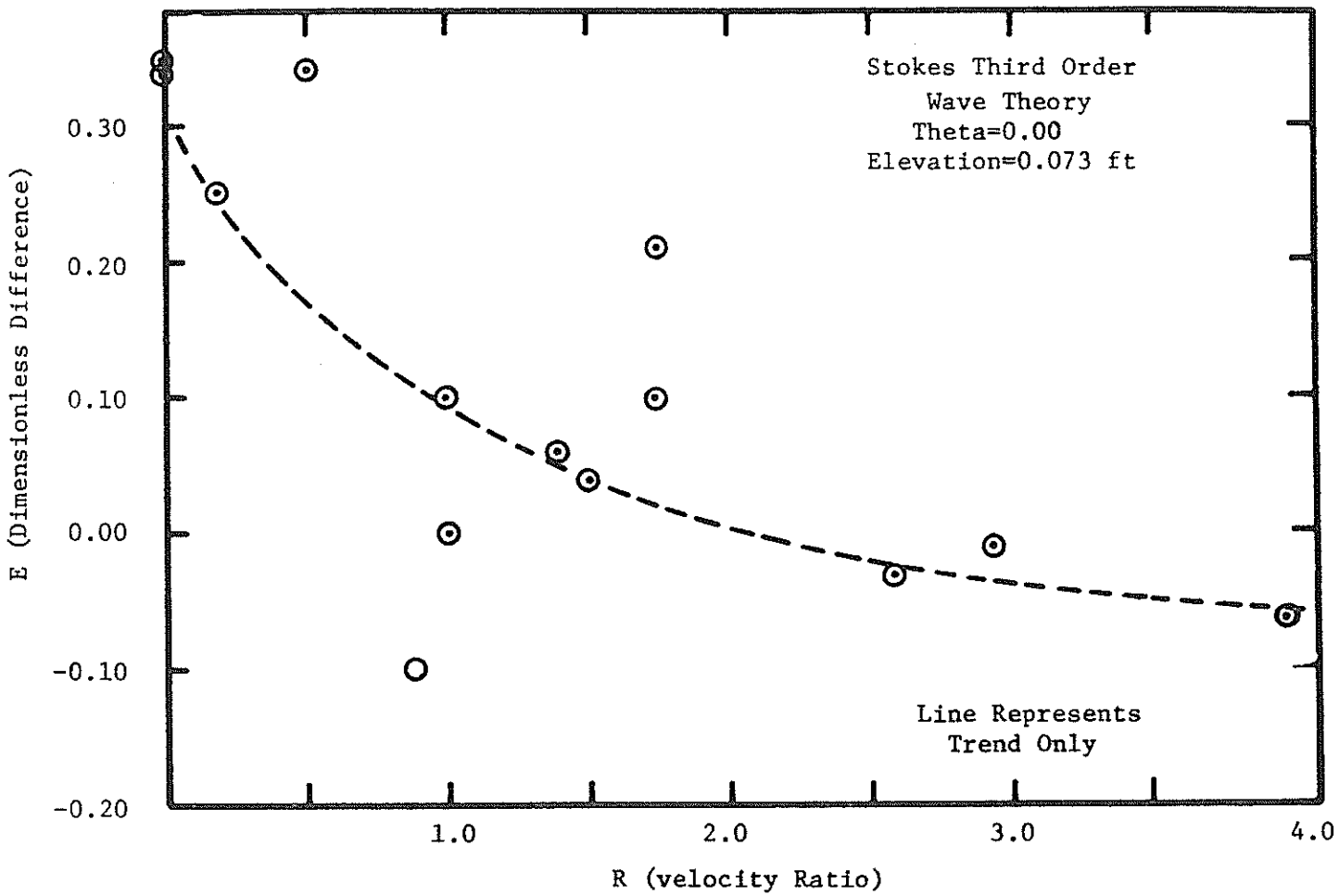

Figure 29 - Dimensionless Difference Versus Velocity Ratio for Stokes Third Order Wave Theory at Elevation 0.073 ft (Theta=0.00)

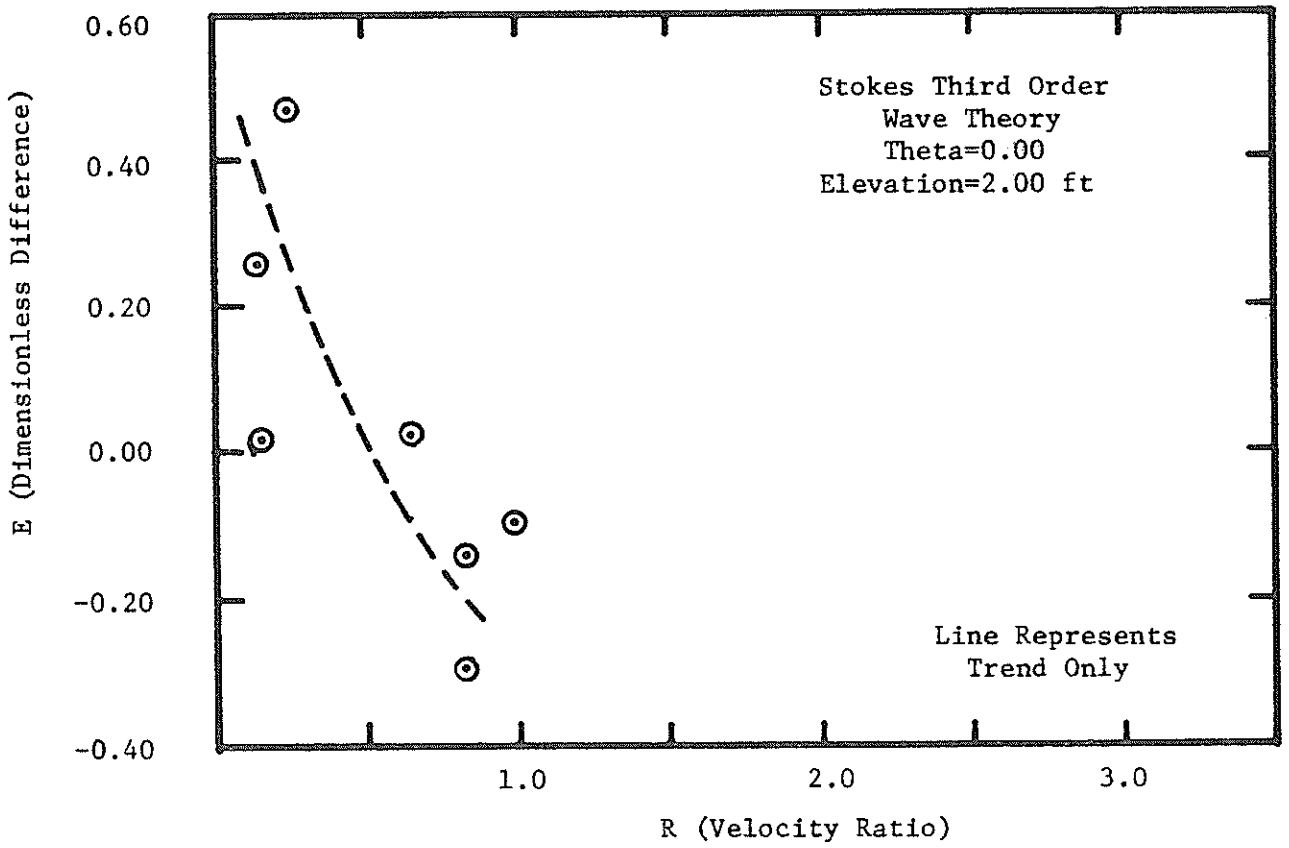

Figure 30 - Dimensionless Difference Versus Velocity Ratio for Stokes Third Order Wave Theory at Elevation 2.00 ft (Theta=0.00)

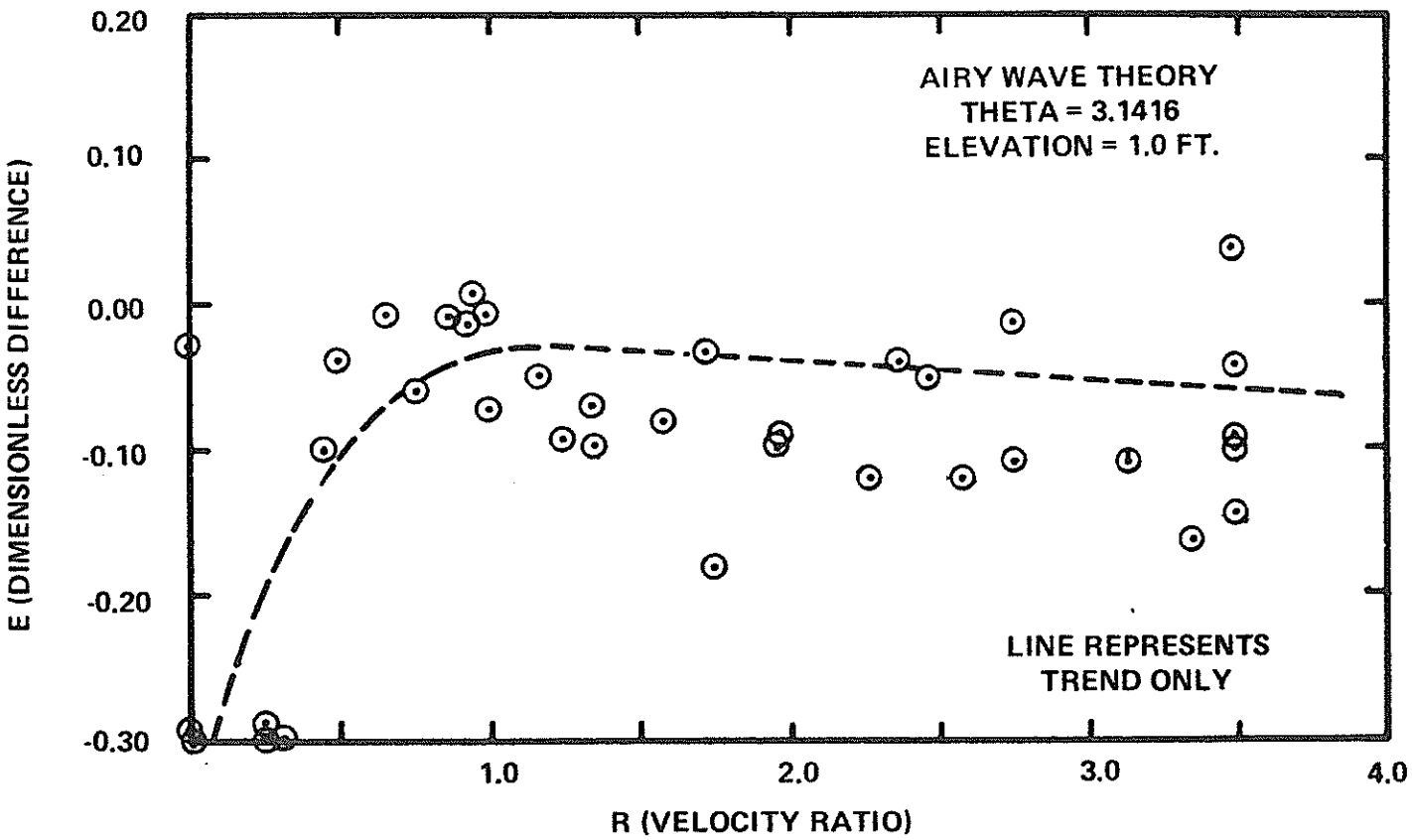

Figure 31 - Dimensionless Difference Versus Velocity Ratio for Airy Wave Theory at Elevation 1.00 ft (Theta=3.1416)

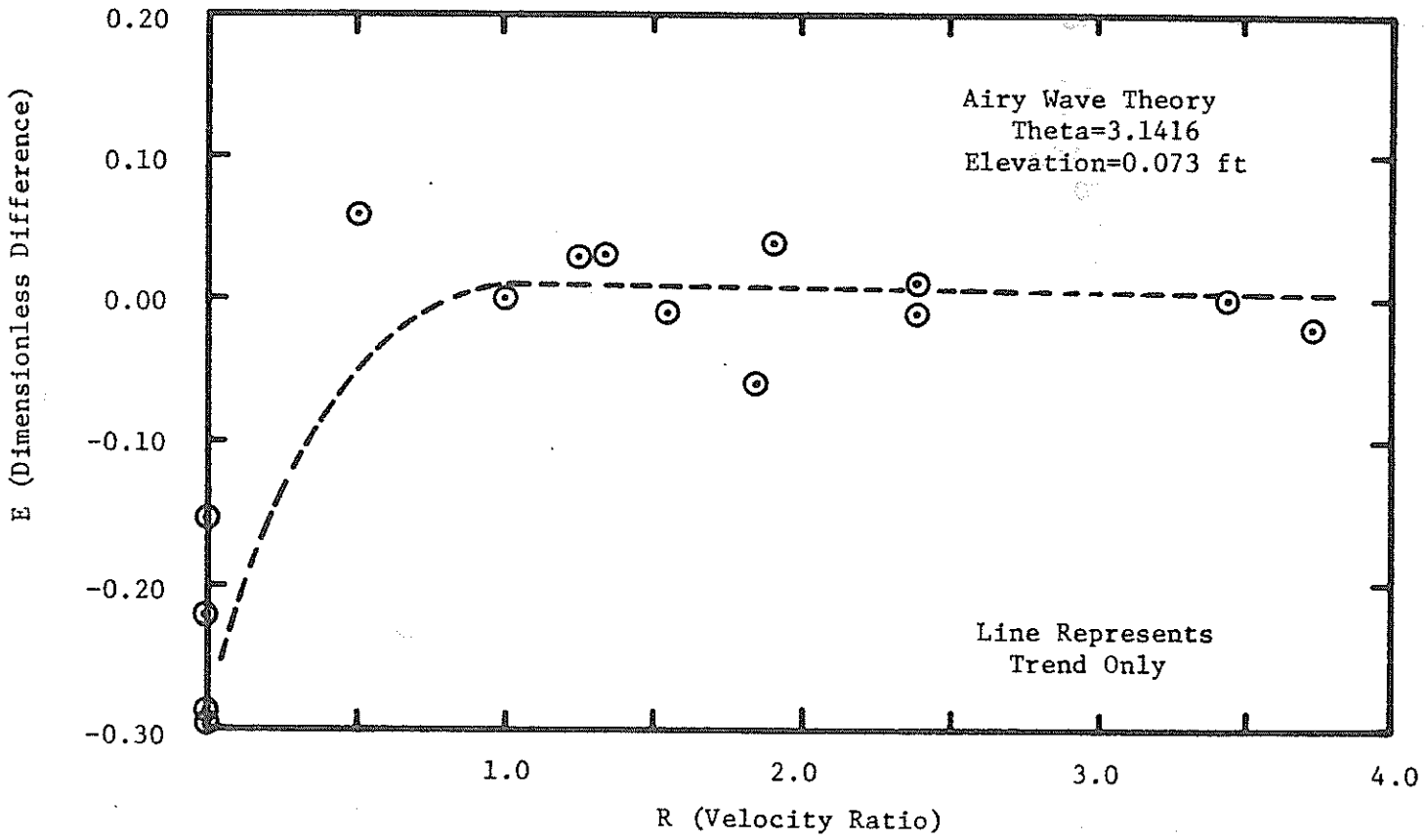

Figure 32 - Dimensionless Difference Versus Velocity Ratio for Airy Wave Theory at Elevation 0.073 ft (Theta=3.1416)

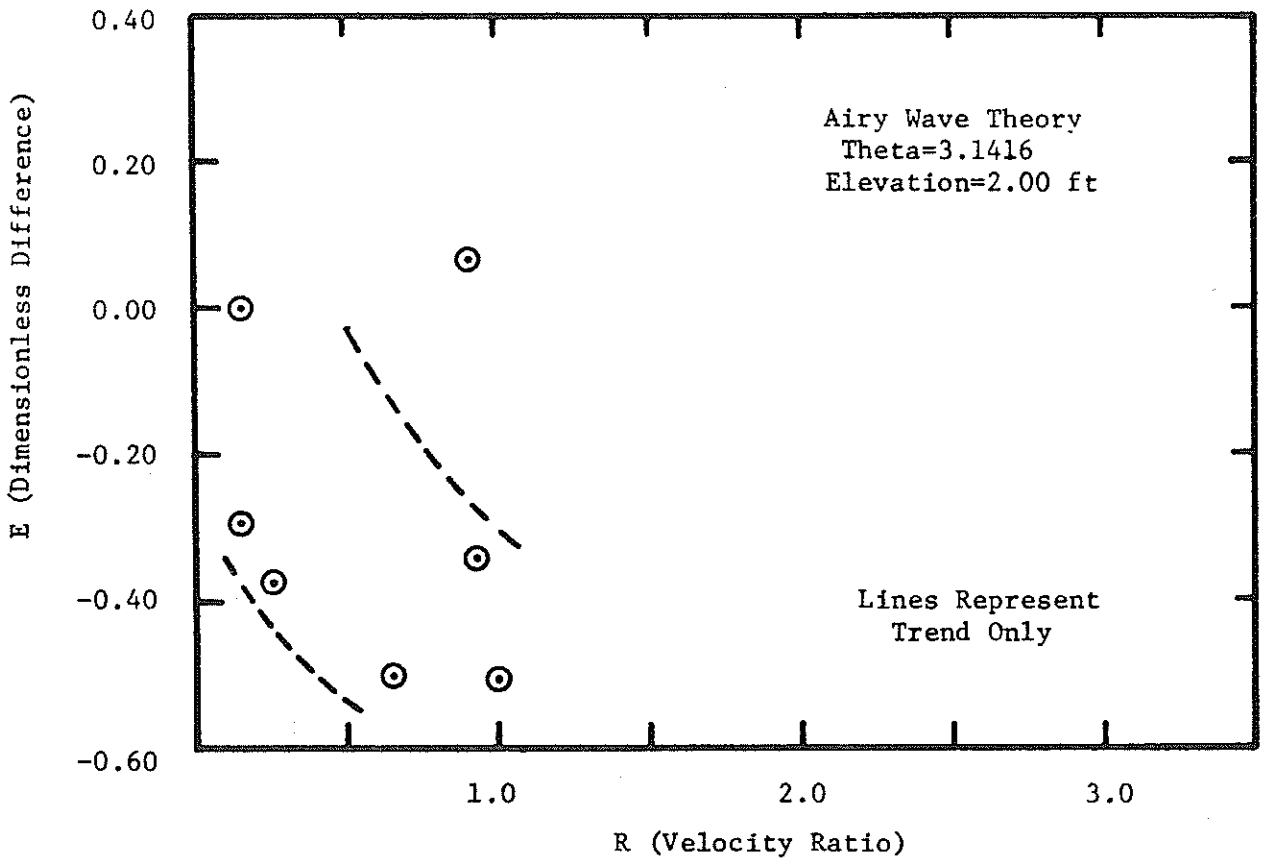

Figure 33 - Dimensionless Difference Versus Velocity Ratio for Airy Wave Theory at Elevation 2.00 ft (Theta=3.1416)

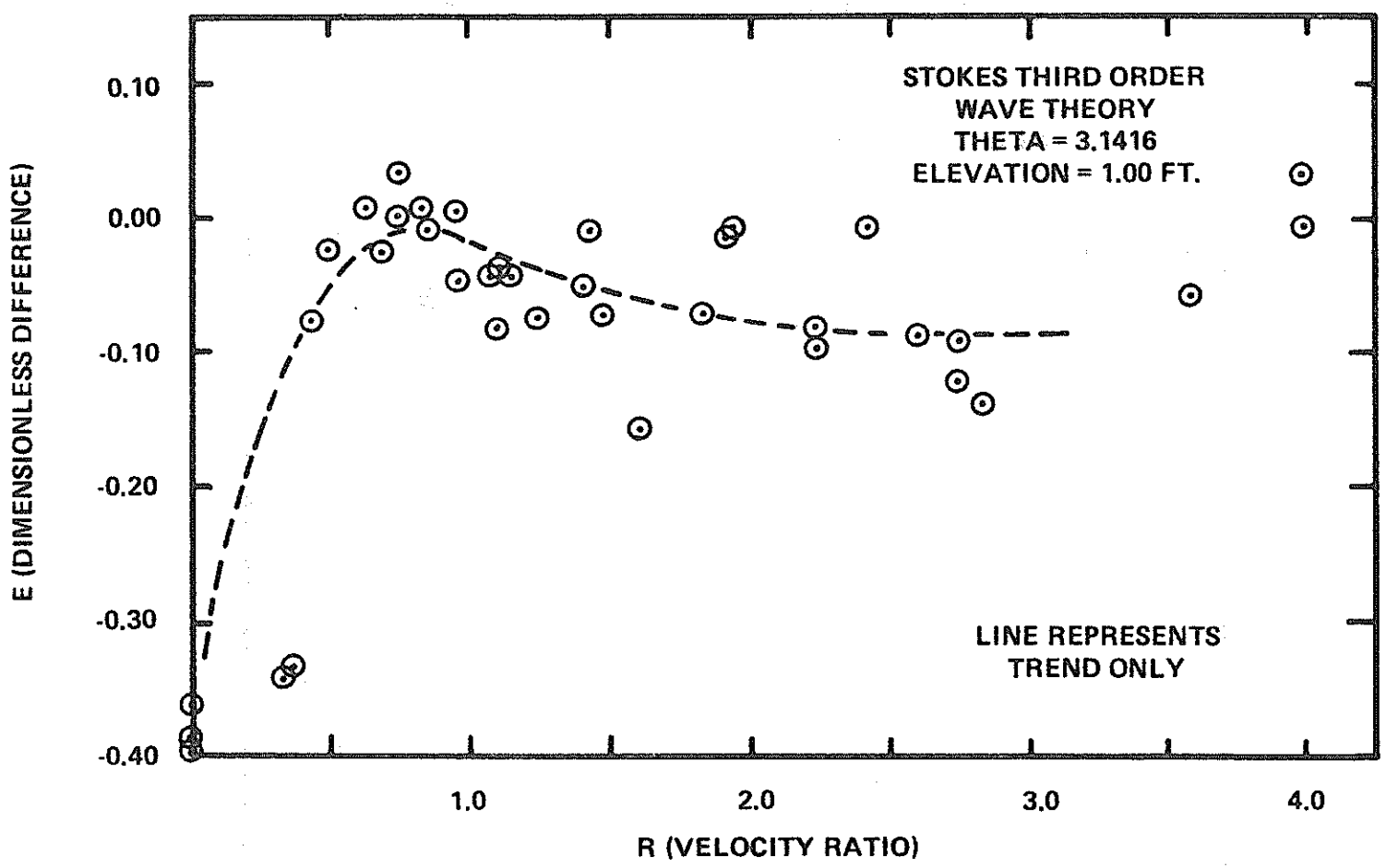

Figure 34 - Dimensionless Difference Versus Velocity Ratio for Stokes Third Order Wave Theory at Elevation 1.00 ft (Theta=3.1416)

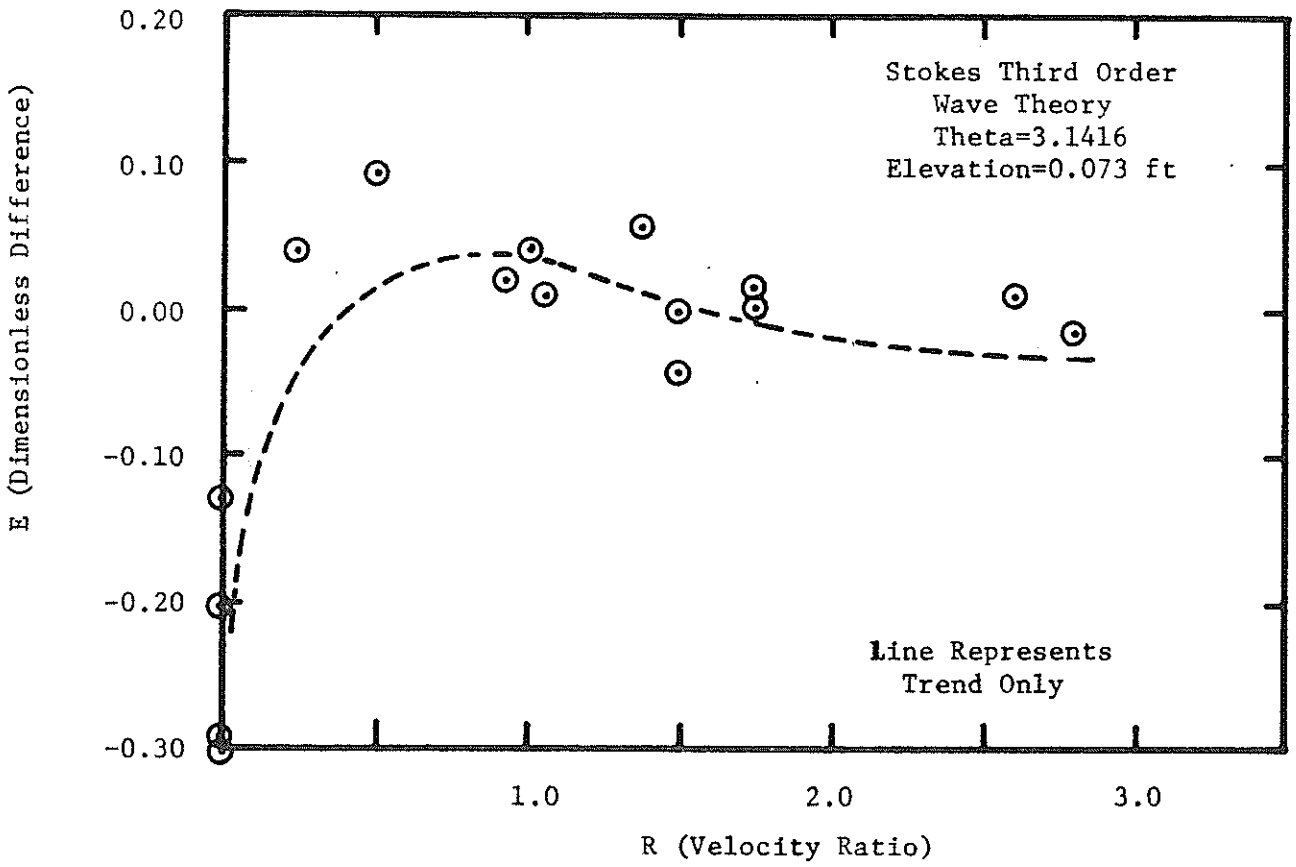

Figure 35 - Dimensionless Difference Versus Velocity Ratio for Stokes Third Order Wave Theory at Elevation 0.073 ft (Theta=3.1416)

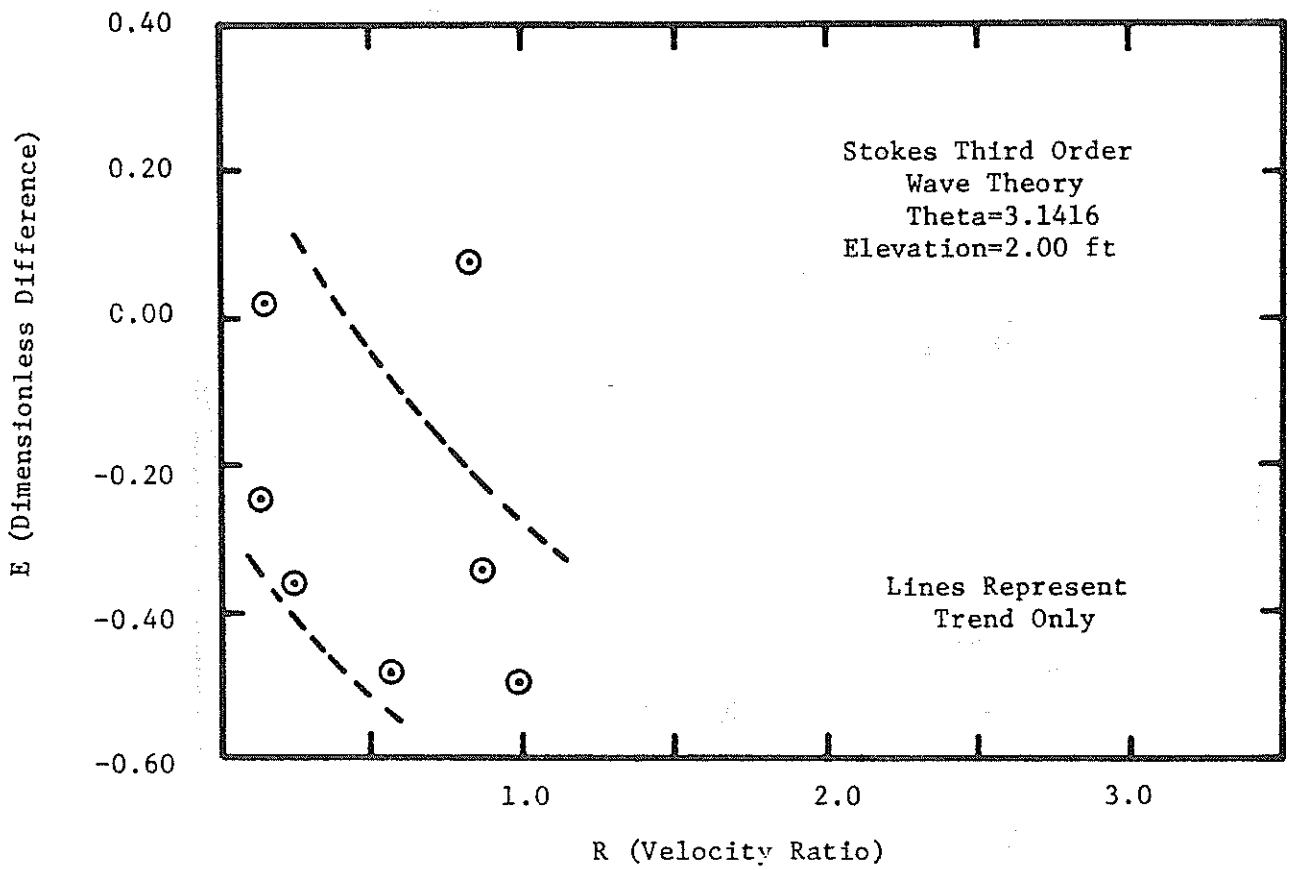

Figure 36 - Dimensionless Difference Versus Velocity Ratio for Stokes Third Order Wave Theory at Elevation 2.00 ft (Theta=3.1416)

A slight tendency exists for Stokes third order wave theory to predict the superimposed velocity better than the Airy prediction. This can be seen by the mean error which is closer to the zero error line.

The fluid force data were analyzed at the crest (data point one) to determine the coefficient drag. At this point the acceleration is equal to zero and only the drag force is present. The coefficients of drag were determined by three methods. The first method used simultaneous measurements of the horizontal fluid force and velocity.

Kim and Hubbard[25] state that "In the past, calculation of C_D from wave force measurements was based on inferred particle velocity from wave elevation. A drawback of this approach is that steady current velocity associated with wave-induced velocity cannot be explicity accounted for, in spite of various approximations by different wave theories to calculate particle velocities."

The second and third methods are based on the predicted velocities of the superposition principle using Airy and Stokes third order wave theories to calculate the coefficient of drag. A comparison of the three methods is made to demonstrate the differences in the coefficient of drag.

The coefficient of drag is related to the Reynolds Number (N_R) and the Keulegan-Carpenter number (N_{KC}) as discussed previously. The coefficient of drag is plotted as a function of the Reynolds number in Figure 37 as computed by the simultaneous measurements of fluid force and fluid velocity; Figure 38 as computed using the superposition principle with Airy wave theory; and Figure 39 as computed using Stokes third order wave theory. Similar plots for the coefficient of drag versus the Keulegan-Carpenter number are shown in Figure 40 for the simultaneous measurements;

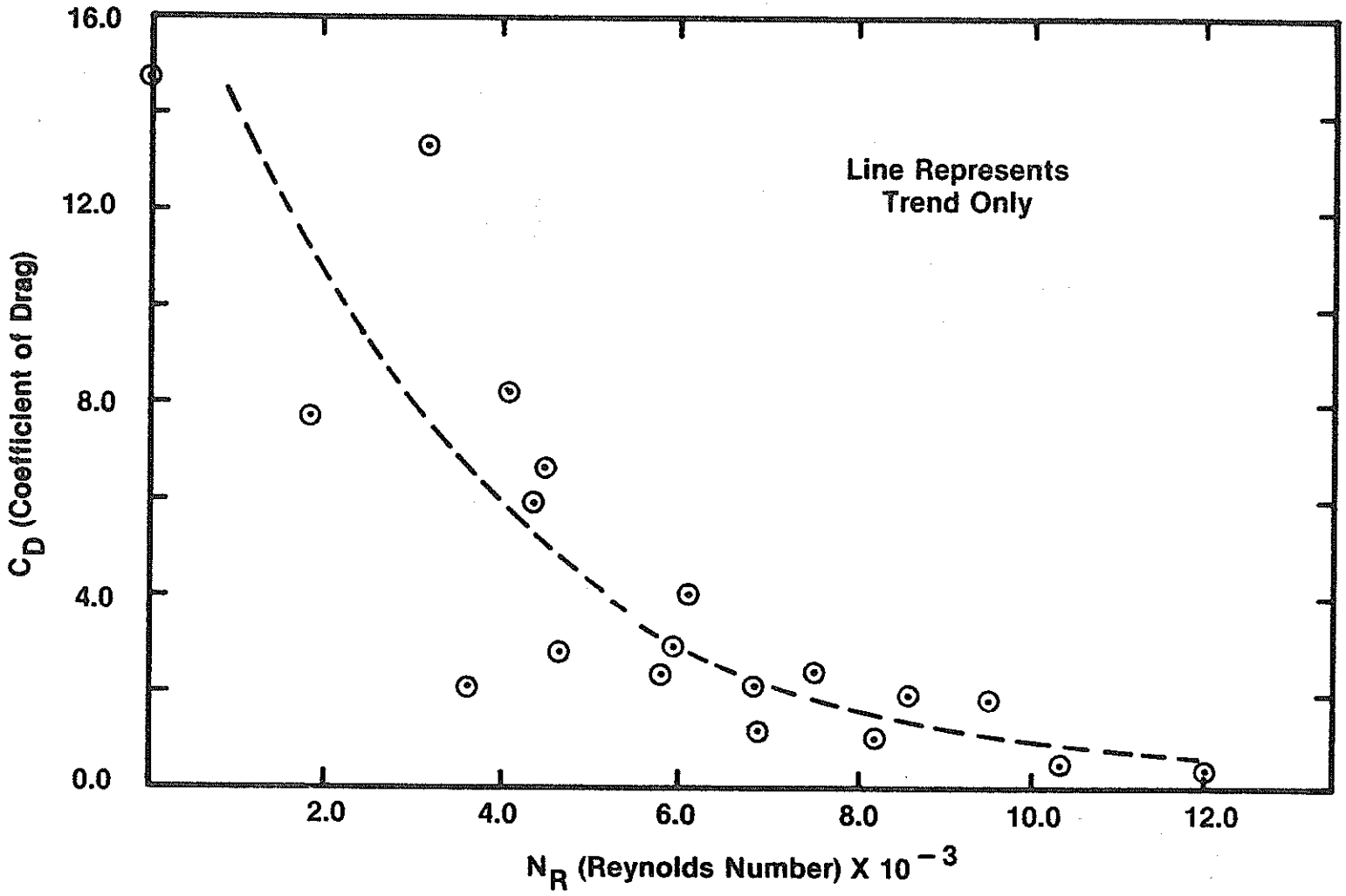

Figure 37 - Coefficient of Drag Versus Reynolds Number
from Simultaneous Force and Velocity Measurements

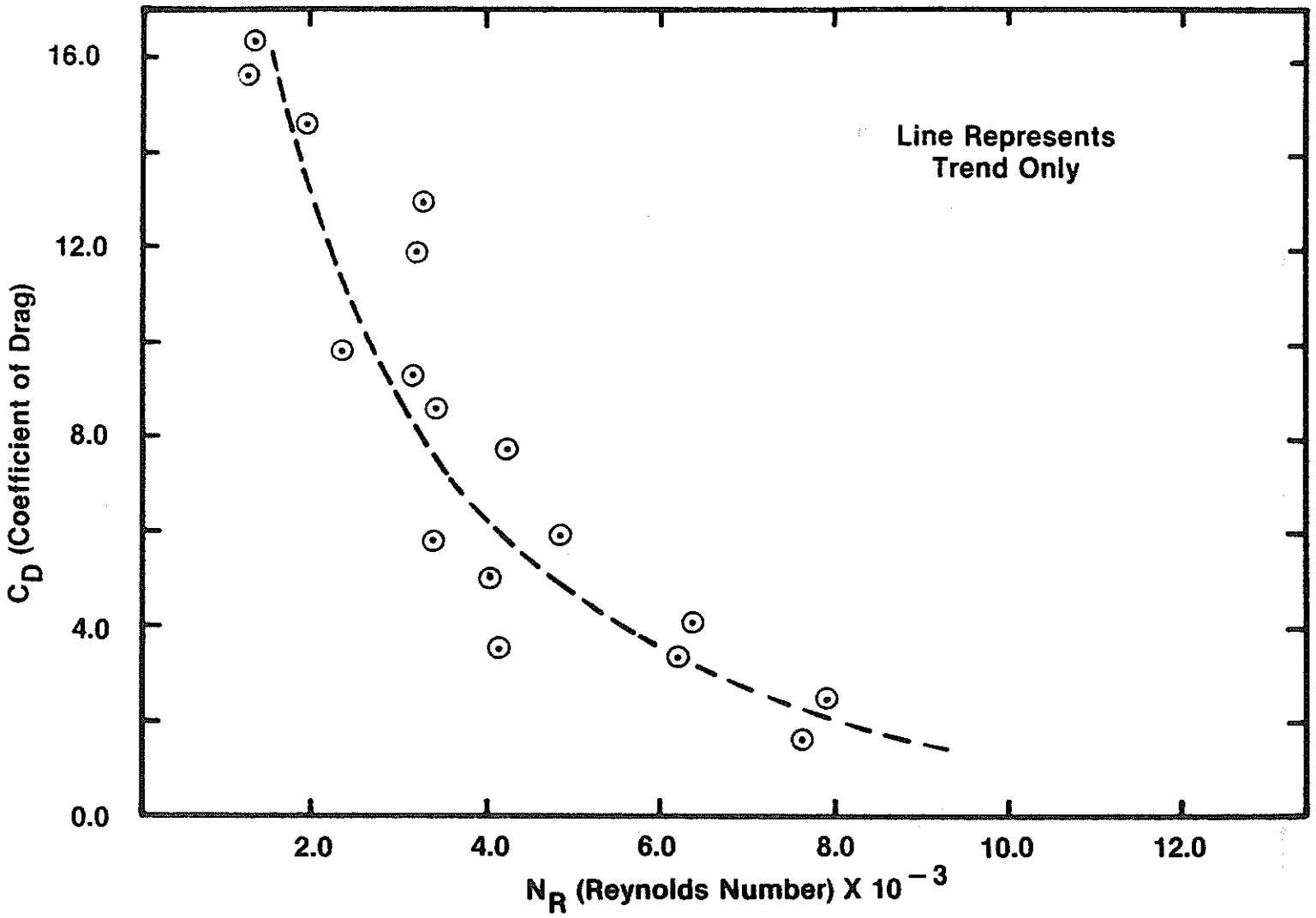

Figure 38 - Coefficient of Drag Versus Reynolds Number from Computations Using Airy Wave Theory

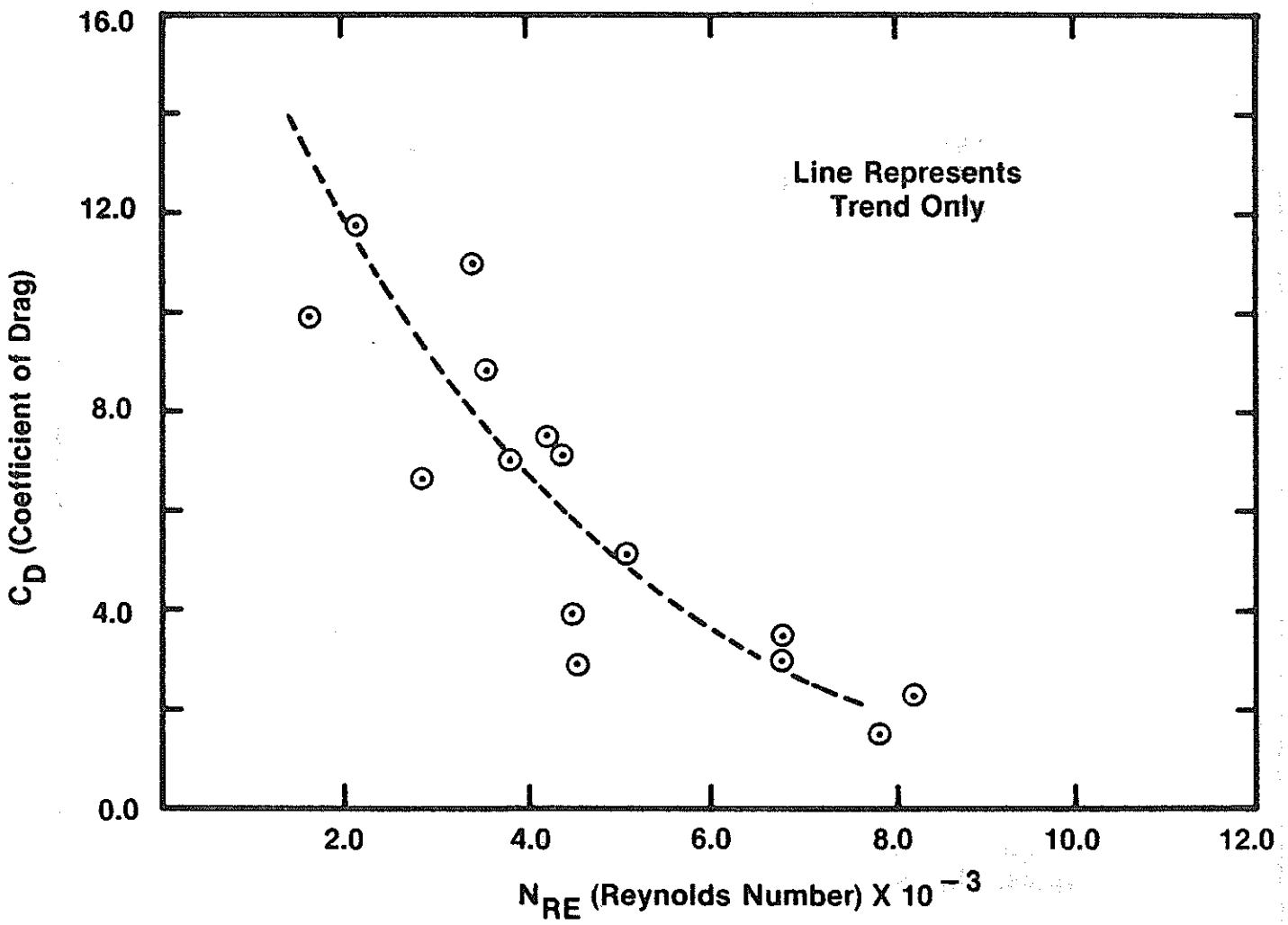

Figure 39 - Coefficient of Drag Versus Reynolds Number
from Computations Using Stokes Third Order Wave Theory

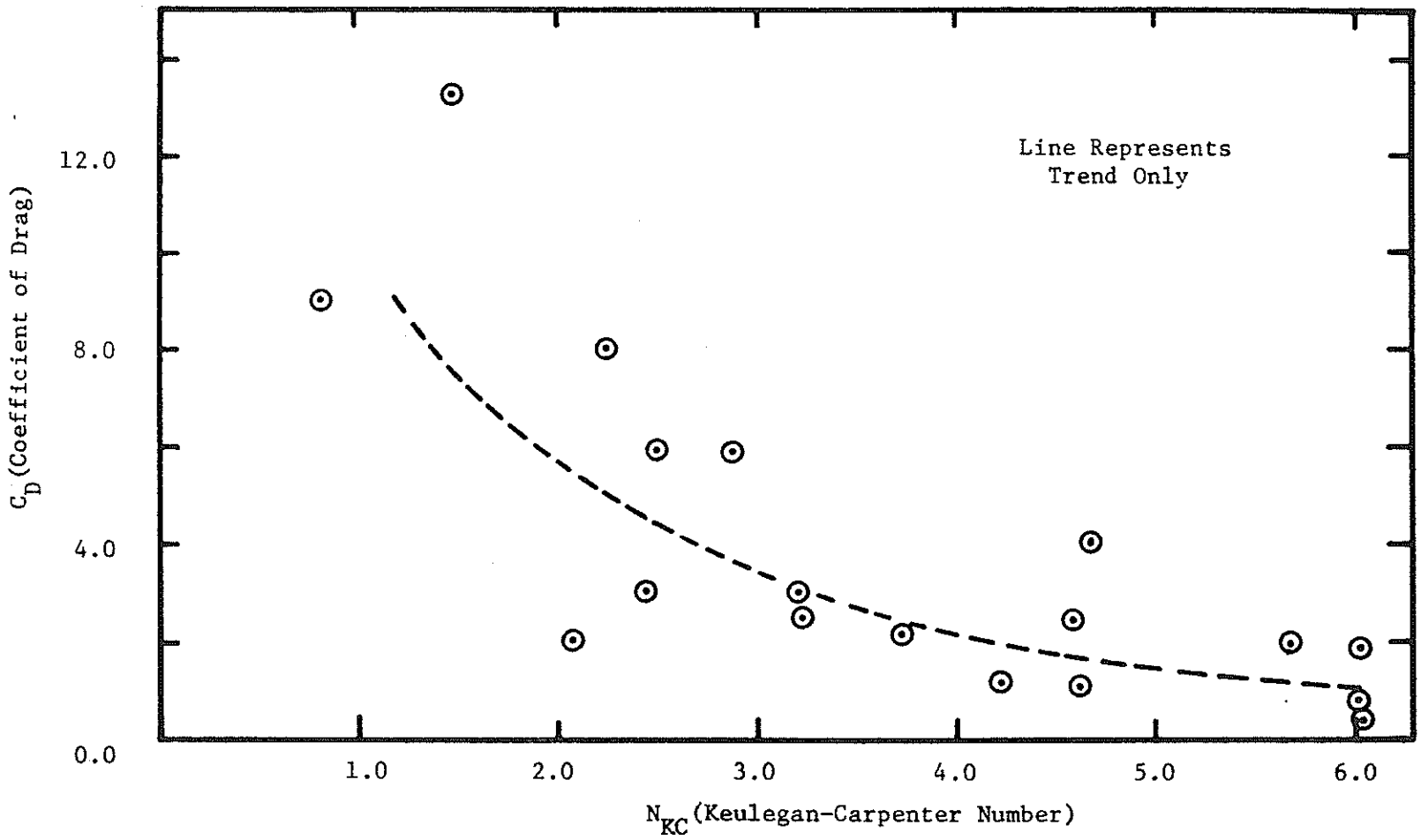

Figure 40 - Coefficient of Drag Versus Keulegan-Carpenter Number from Simultaneous Force and Velocity Measurements

Figure 41 for Airy wave theory; and Figure 42 for Stokes third order wave theory.

These figures all show the same general trend of reduction in the coefficient of drag with increasing Reynolds numbers and Keulegan-Carpenter numbers. The results using the Keulegan-Carpenter number ($\frac{U_{max}}{D}$) seemed to be reversed from results presented previously by other authors. This parameter generally is used to present data over a large range of wave periods (T). However, since the results of this research were for a narrow band of periods, the change in the velocity (U_{max}) is more predominant than the change in period (T). Both the Reynolds number and Keulegan-Carpenter number are attached by the increasing velocity and exhibit the same trend.

Figures 37 to 39 show that the coefficient of drag is less when computed from the measured velocity as opposed to the Airy or Stokes III velocities for the range of Reynolds numbers shown. This is related to the fact that the wave theories used in conjunction with the superposition principle have a tendency to under predict the horizontal velocity near the bottom boundary as demonstrated by Figures 26 and 29 (pp. 61 and 63).

The relative difference between the coefficients of drag computed by Airy wave theory and these computed by measured values are shown in Figure 43. This figure demonstrates that at low velocity ratios (R) the coefficients computed using Airy wave theory are greater than the actual values, but this difference decreases with increasing currents.

The coefficients of drag computed by the simultaneous measurements of the horizontal fluid force and velocity are, by definition, the actual values. These coefficients can only be used if the actual horizontal velocity can be predicted. This supports the fact that the coefficients

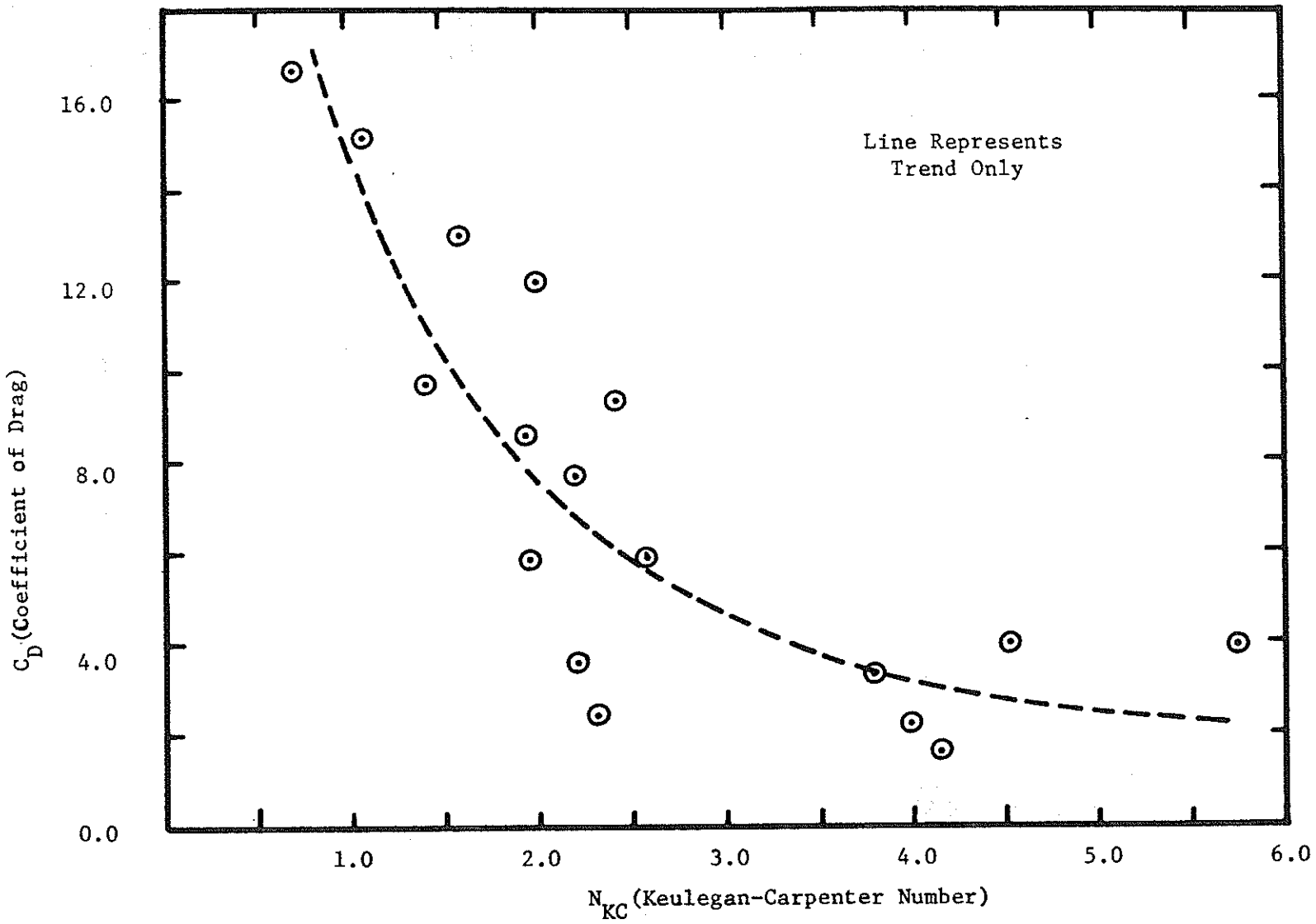

Figure 41 - Coefficient of Drag Versus Keulegan-Carpenter Number from Computations Using Airy Wave Theory

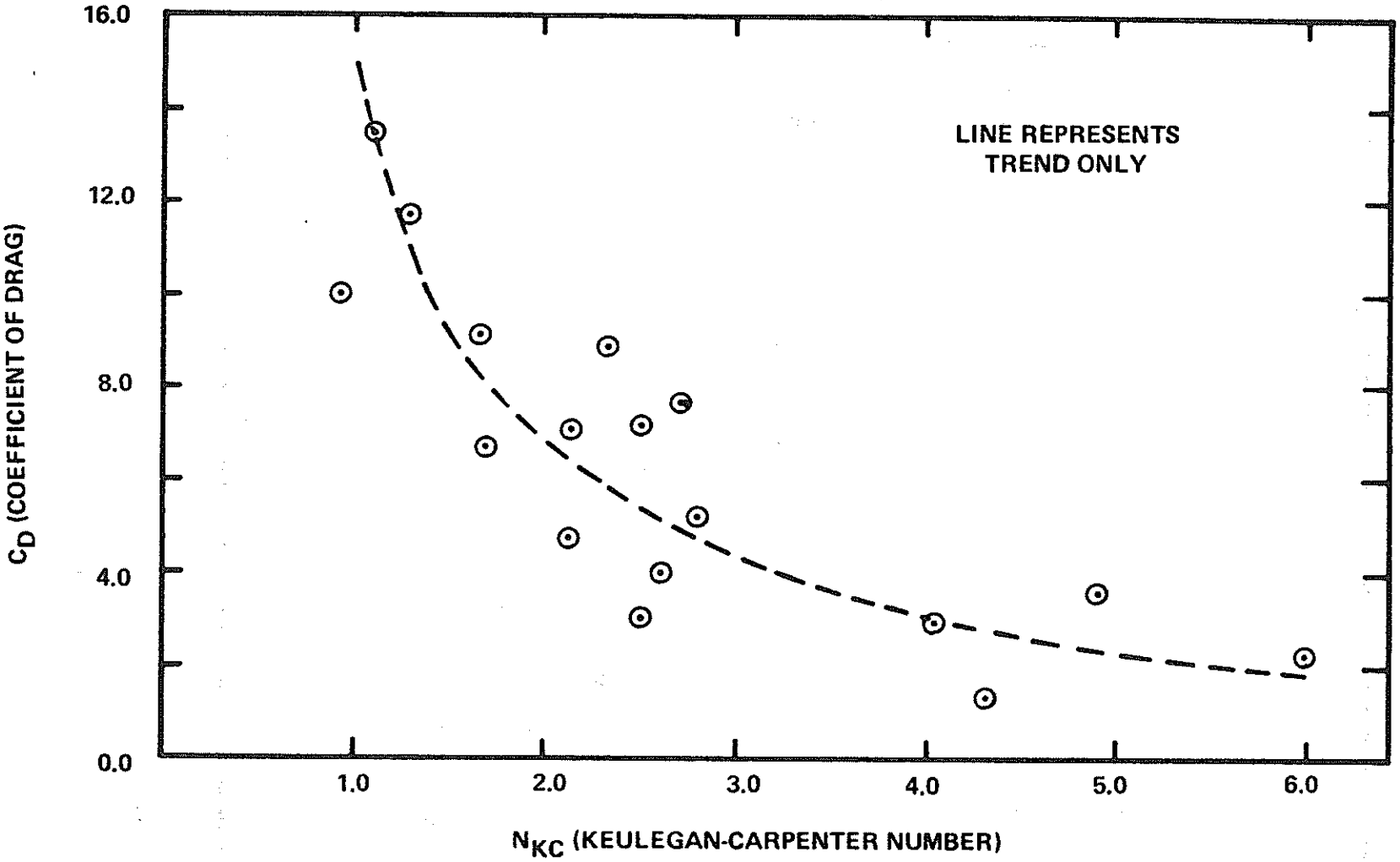

Figure 42 - Coefficient of Drag Versus Keulegan-Carpenter Number from Computations Using Stokes Third Order Wave Theory

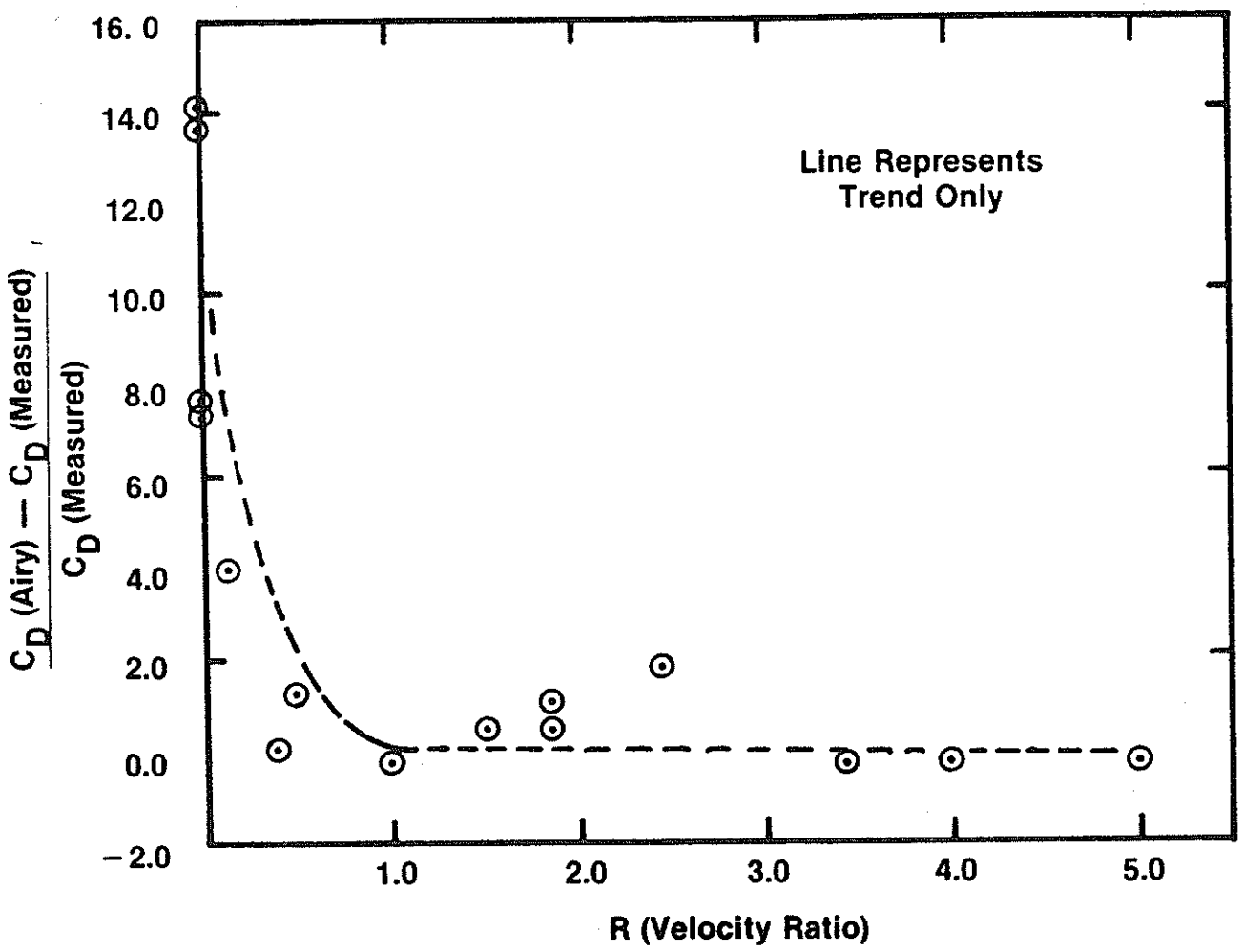

Figure 43 - Relative Difference of C_D for Airy Wave Theory and Measured Values Versus the Velocity Ratio

of drag are dependent on the method used to determine the horizontal velocity. Therefore, the prediction of forces on a cylinder should be consistent with the method which was used to determine the coefficients.

Figure 44 shows the actual coefficient of drag for the horizontal cylinder for the steady-state current condition.

A small diameter test cylinder was needed to fulfill the assumption of two-dimensional flow. A drawback of the small cylinder was that the drag forces were small and the inertia forces were approaching zero. The measuring device of this research was developed to determine the small forces. However, during the testing, an inertial force of the same order of magnitude as the drag forces was found in phase with the fluid acceleration due to the inertia of the measuring device. This inertial force overshadowed that of the added mass effect and therefore the coefficient of added mass could not be determined.

Normally for an inertia-dominated test specimen, the order of magnitude of the total measured force is much greater than the inertia force due to the measuring device, and the error of the device can be neglected.

The primary purpose of this research was to determine the drag forces associated with the horizontal velocity. These drag forces were determined when the velocity was maximum and the acceleration was zero. Therefore, no inertial effects were present and the coefficient of drag was unaltered by this effect.

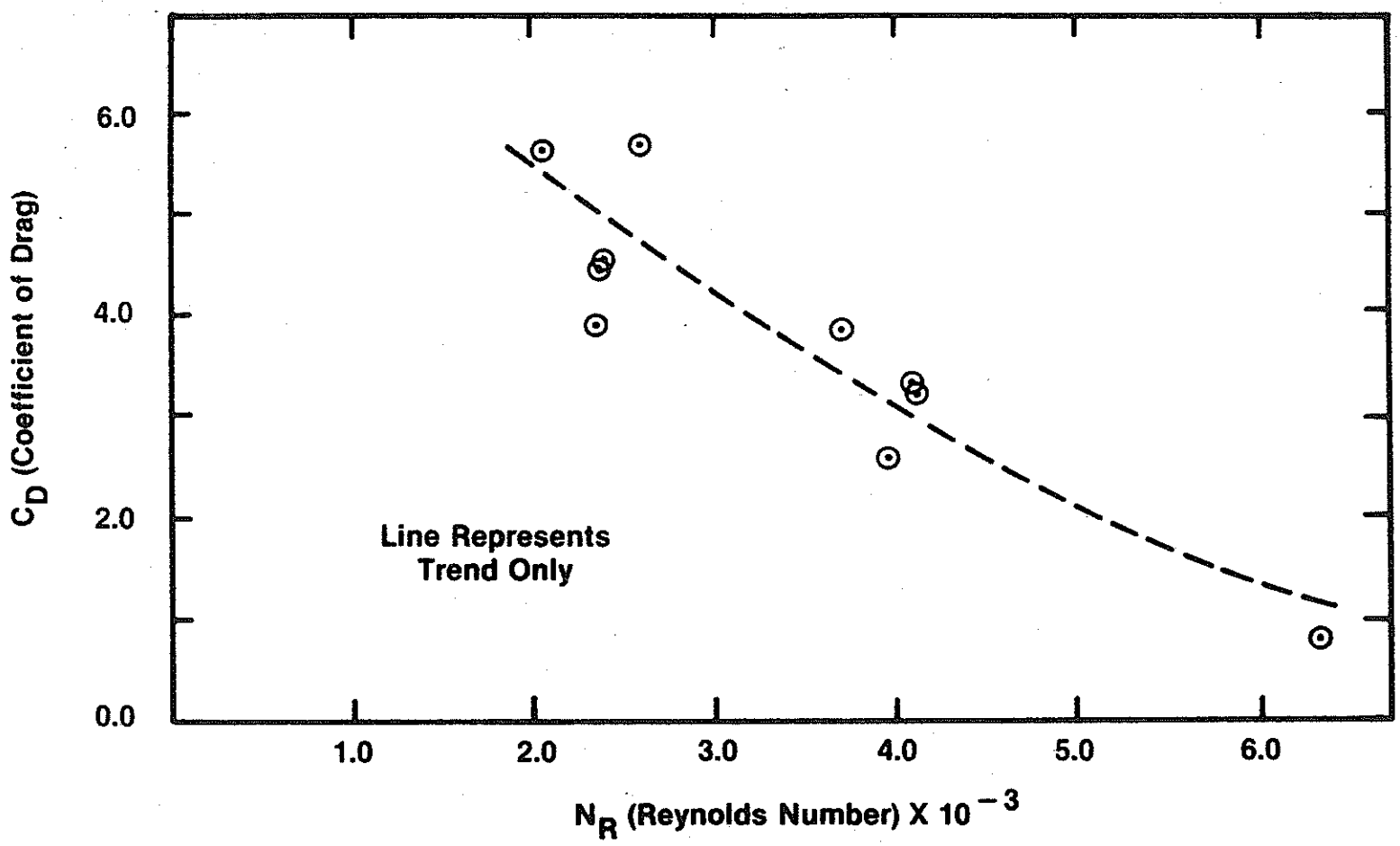

Figure 44 - Coefficient of Drag Versus Reynolds Number (Steady-State Current Condition)

CONCLUSIONS AND RECOMMENDATIONS

The primary objective of this research was to investigate the effect of a current on the horizontal velocity field of a surface gravity wave and the related fluid force on a horizontal cylinder near the bottom boundary. This objective was accomplished by a model testing program in which simultaneous waves and currents were present. The superposition principle was used with the horizontal velocity fields of the wave and current to predict the combined field. Since this assumption is not valid for nonuniform currents, the error associated with this assumption was determined.

The following conclusions were evident from the testing program for the range of values tested.

1. Airy and Stokes third order wave theories in conjunction with the superposition principle predict the horizontal velocity reasonably well for velocity ratios ($R = \frac{U}{u}$) greater than one. For values less than one the velocities are under predicted. The validity of superposition principle is further reduced near the bottom boundary for the higher velocity ratios.
2. The coefficients of drag computed from Airy and Stokes third order wave theories in conjunction with the superposition principle are greater in magnitude than the values determined by the simultaneous force and velocity measurement. This difference decreases with increasing velocity ratios.

The conclusions were based on a limited testing program. These

results can be extended over a greater range of waves and currents by further tests. These additional tests will indicate whether any scale effects are important.

Other conditions related to the pipeline problem such as the distance of the cylinder from the boundary, the transverse (lift) force, relative roughness and orientation angles should be investigated for the combined wave-current condition.

Other theories developed for the interaction of waves and currents should be tested experimentally to determine their accuracy for the prediction of fluid force and particle kinematics.

In summary, the existing knowledge of wave forces should be expanded to include the effect of a simultaneous current. This research only scratches the surface of the knowledge needed to understand the wave-current problem.

REFERENCES

1. Morison, J. R., et al., "The Force Exerted by Surface Waves on Piles," Petroleum Transactions, American Institute of Mining, Metallurgical, and Petroleum Engineering, Vol. 189, 1950, pp. 149-154.

2. Longuet-Higgins, M. S., and Stewart, R. W., "Changes in the Form of Short Gravity Waves on Long Waves and Tidal Currents," Journal of Fluid Mechanics, Vol. 8, 1960, pp. 565-583.

3. Longuet-Higgins, M. S., and Stewart, R. W., "The Changes in Amplitude of Short Gravity Waves on Steady Non-Uniform Currents," Journal of Fluid Mechanics, Vol. 10, 1961, pp. 529-549.

4. Jonsson, I. G., Skougaard, C., and Wang, J. D., "Interaction Between Waves and Currents," Proceedings of the Coastal Engineering Conference, 1970, Vol. 1, pp. 489-507.

5. Hales, L. Z., and Herbich, J. B., "Effects of a Steady Non-Uniform Current on the Characteristics of Surface Gravity Waves," U.S. Army Engineer Waterways Experiment Station, Miscellaneous Report H-74-11, December 1974, 186 pages.

6. Dalrymple, Robert A., "Waves and Wave Forces in the Presence of Currents," Civil Engineering in the Oceans, 1970, Vol. 2, pp. 999-1018.

7. Tung, C. C., and Huang, N. E., "Combined Effects of Currents and Waves on Fluid Force," Ocean Engineering, Vol. 2, 1973, pp. 183-193.

8. Tung, C. C., and Huang, N. E., "Influence of Wave-Current Interactions on Fluid Force," Ocean Engineering, Vol. 2, 1973, pp. 207-218.

9. Unna, P. J. H., "Waves and Tidal Streams," Nature, Vol. 149, 1942, p. 219.

10. Peregrine, D. H., "Interaction of Water Waves and Currents," Advances in Applied Mechanics, Vol. 16, 1976, pp. 10-111.

11. Dalrymple, Robert A., "Models for Nonlinear Water Waves on Shear Currents," Offshore Technology Conference, 1974, Paper No. 2114.

12. Dean, R. G., "Stream Function Representation of Nonlinear Ocean Waves," Journal of Geophysical Research, Vol. 70, No. 18, September 15, 1965.

13. Sarpkaya, T., "Oscillatory Gravity Waves in Flowing Water," Transactions of the American Society of Civil Engineers, Vol. 122, 1957, pp. 564-586.

14. Herbich, J. B., Ziegler, J., and Bowers, C. E., "Experimental Studies of Hydraulic Breakwaters," Project Report No. 51, St. Anthony Falls Hydraulic Laboratory, University of Minnesota, 1956, 109 pages.

15. Aagaard, P. M., and Dean, R. G., "Wave Forces: Data Analysis and Engineering Calculation Methods," Offshore Technology Conference, Paper No. 1008, 1969.

16. Tung, C. C., and Huang, N. E., "Influence of Current on Statistical Properties of Waves," Journal of the Waterways, Harbors and Coastal Engineering Division, Vol. 100, 1974, pp. 267-278.

17. Wu, S. C., and Tung, C. C., "Structural Response to Wave and Current Forces," Civil Engineering in the Oceans, Vol. 2, 1975, pp. 849-864.

18. Malhotra, A. K., and Penzien, J., "Nondeterministic Analysis of Offshore Structures," Journal of the Engineering Mechanics Division, American Society of Civil Engineers, Vol. 96, No. EM6, 1970, pp. 985-1003.

19. Sekita, K., "Laboratory Experiments on Wave and Current Forces Acting on a Fixed Platform," Offshore Technology Conference, 1975, Paper No. 2191.

20. David, D. A., and Ciani, J. B., "Wave Forces on Submerged Pipelines - A Review with Design Aids," Naval Facilities Engineering Command, Technical Report No. R844, July 1976, 55 pages.

21. Keulegan, G. H., and Carpenter, L. H., "Forces on Cylinders and Plates in an Oscillating Fluid," Journal of Research of the National Bureau of Standards, Vol. 60, No. 5, 1958, pp. 423-440.

22. Garrison, C. J., and Rao, U. S., "Interaction of Waves With Submerged Objects," Journal of the Waterways, Harbors and Coastal Engineering Division, American Society of Civil Engineers, Vol. 97, No. WW2, May 1971, pp. 259-277.

23. Airy, G. B., "On Tides and Waves," Encyclopedia Metropolitanna, London, 1842, p. 289.

24. Skjelbreia, L., "Gravity Waves: Stokes Third Order Approximation, Tables of Functions," Council on Wave Research, The Engineering Foundation, 1959, p. 336.

25. Kim, Y. Y.,, and Hibbard, H. C., "Analysis of Simultaneous Wave Force and Water Particle Velocity Measurements," Offshore Technology Conference, 1975, Paper No. 2192.